J. Fluid Mech. (1997), *vol.* 347, *pp.* 197–234. Printed in the United Kingdom

Turbulence, waves and mixing at shear-free density interfaces. Part 1. A theoretical model

By H. J. S. FERNANDO[1]† AND J. C. R. HUNT[2]‡

[1]Environmental Fluid Dynamics Program, Department of Mechanical and Aerospace Engineering, Arizona State University Tempe, AZ 85287-6106, USA

[2]Meteorological Office, London Road, Bracknell, Berkshire RE12 2SZ, UK

(Received 2 February 1996 and in revised form 19 May 1997)

This paper presents a theoretical model of turbulence and mixing at a shear-free stable density interface. In one case (single-sided stirring) the interface separates a layer of fluid of density ρ in turbulent motion, with r.m.s. velocity u_H and lengthscale L_H, from a non-turbulent layer with density $\rho + \Delta\rho$, while in the second case (double-sided stirring) the lower layer is also in turbulent motion. In both cases, the external Richardson number $Ri = \Delta b L_H / u_H^2$ (where Δb is the buoyancy jump across the interface) is assumed to be large. Based on the hypotheses that the effect of the interface on the turbulence is as if it were suddenly imposed (which is equivalent to generating irrotational motions) and that linear waves are generated in the interface, the techniques of rapid distortion theory are used to analyse the linear aspects of the distortion of turbulence and of the interfacial motions. New physical concepts are introduced to account for the nonlinear aspects.

To describe the spectra and variations of the r.m.s. fluctuations of velocity and displacements, a statistically steady linear model is used for frequencies above a critical frequency ω_r/μ_c, where $\omega_r (= \Delta b/2u_H)$ is the maximum resonant frequency and $\mu_c < 1$. As in other nonlinear systems, observations below this critical frequency show the existence of long waves on the interface that can grow, break and cause mixing between the two fluid layers. A nonlinear model is constructed based on the fact that these breaking waves have steep slopes (which determines the form of the displacement spectrum) and on the physical argument that the energy of the vertical motions of these dissipative nonlinear waves should be comparable to that of the forced linear waves, which leads to an approximately constant value for the parameter μ_c. The model predictions of the vertical r.m.s. interfacial velocity, the interfacial wave amplitude and the velocity spectra agree closely with new and published experimental results.

An exact unsteady inviscid linear analysis is used to derive the growth rate of the full spectrum, which asymptotically leads to the growth of resonant waves and to the energy transfer from the turbulent region to the wave motion of the stratified layer. Mean energy flux into the stratified layer, averaged over a typical wave cycle, is used to estimate the boundary entrainment velocity for the single-sided stirring case and the flux entrainment velocity for the double-sided stirring case, by making the assumption that the ratio of buoyancy flux to dissipation rate in forced stratified layers is constant with Ri and has the same value as in other stratified turbulent flows. The calculations are in good agreement with laboratory measurements conducted in mixing boxes and in wind tunnels. The contribution of Kelvin–Helmholtz instabilities

† Author to whom correspondence should be addressed (e-mail: J.Fernando@asu.edu).

‡ Present address: Department of Applied Mathematics and Theoretical Physics, University of Cambridge, Silver Street, Cambridge CB3 9EW, UK.

induced by the velocity of turbulent eddies parallel to the interface is estimated to be insignificant compared to that of internal waves excited by turbulence.

1. Introduction

Turbulent mixing at a shear-free density interface is a crucial process for determining the dynamical states of well-mixed layers in the ocean and atmosphere and also the physical properties and concentrations of chemical and biological constituents in these layers (Fernando 1991; Carruthers & Hunt 1996). When there are no vertical density gradients, turbulence in one region of a flow spreads into contiguous regions as the eddies randomly induce each other to fill the available space. However, in the presence of a layer where the fluid is stably stratified, the buoyancy forces inhibit this motion and the rate of spreading is greatly reduced. Figure 1(*a*) shows a typical stratified fluid system forced by the turbulence in region 1. Below the turbulent layer, in the stably stratified region (region 2) of thickness h, the buoyancy frequency is $N_2 = (\Delta b/h)^{1/2}$, where Δb is the buoyancy jump across this layer. (The buoyancy is defined as $b = (\rho_0 - \rho)g/\rho_0$, where ρ is the density of the fluid, ρ_0 is the reference density and g is the gravitational acceleration). Region 2 is also commonly called the inversion layer or the interfacial layer, within which nonlinear dissipative wave-like motions are prevalent. In many geophysical situations, stratification in region 2 is sufficiently great that motions within it are non-turbulent, but are coupled with the turbulence in region 1. The flow field on the other side of the interface (region 3) may either be turbulent (so that the form of velocity field $u_{(3)}$ is $\mathscr{T}$) or non-turbulent. These non-turbulent motions may take the form of wave motions driven by interfacial motions (i.e. $u_{(3)}$ is $\mathscr{W}$), if region 3 is stably stratified, or irrotational (potential flow) motions, if region 3 is unstratified ($u_{(3)}$ is I).

Carruthers & Hunt (1986) have studied the case with $\Delta b = h = 0$ and $u_{(3)} = \mathscr{W}$, which was later extended to include the presence of a thick interface with $\Delta b \neq 0$ (Carruthers & Hunt 1997). The latter case is a good approximation for atmospheric inversion layers in the presence of convective turbulence (Deardorff 1980; Lenschow, Patel & Isbell 1988) and for certain oceanic convectively driven flows. However, there are also many geophysical flows as well as laboratory experiments where the interfacial layer is observed to be thinner than the lengthscale of turbulence while having a significant jump in density across the layer, so that $\Delta b \neq 0$. The present work is aimed towards understanding the interaction between background turbulence and such interfaces. Figure 1(*b*) is a schematic of a thin stratified breaking interface in which mixing is known to occur in isolated patches.

Carruthers & Hunt (1997) have carried out a comprehensive analysis on the nature of the wave field induced at a density interface by a contiguous turbulent layer (also see Carruthers, Hunt & Turfus 1986). They showed that the mode of interfacial oscillations is determined by the *internal Richardson number* $Ri_{(I)}$ of the interface, defined as $Ri_{(I)} = N_2^2 h^2/u_H^2 = \Delta b h/u_H^2$, where u_H is the r.m.s. velocity of region 1. If the interface is thin enough so that $Ri_{(I)} \leqslant \pi^2$, there are no significant motions within it compared with the motion or displacement (ζ) of the interface, thus resulting in the flapping (or the first mode) of internal waves. However, if the *external Richardson number* $Ri = \Delta b L_H/u_H^2$, where L_H is the integral length scale of region 1, is large enough the interface has a significant dynamical influence on the external turbulence. In some cases the thickness h and $Ri_{(I)}$ are great enough ($\geqslant \pi^2$) that

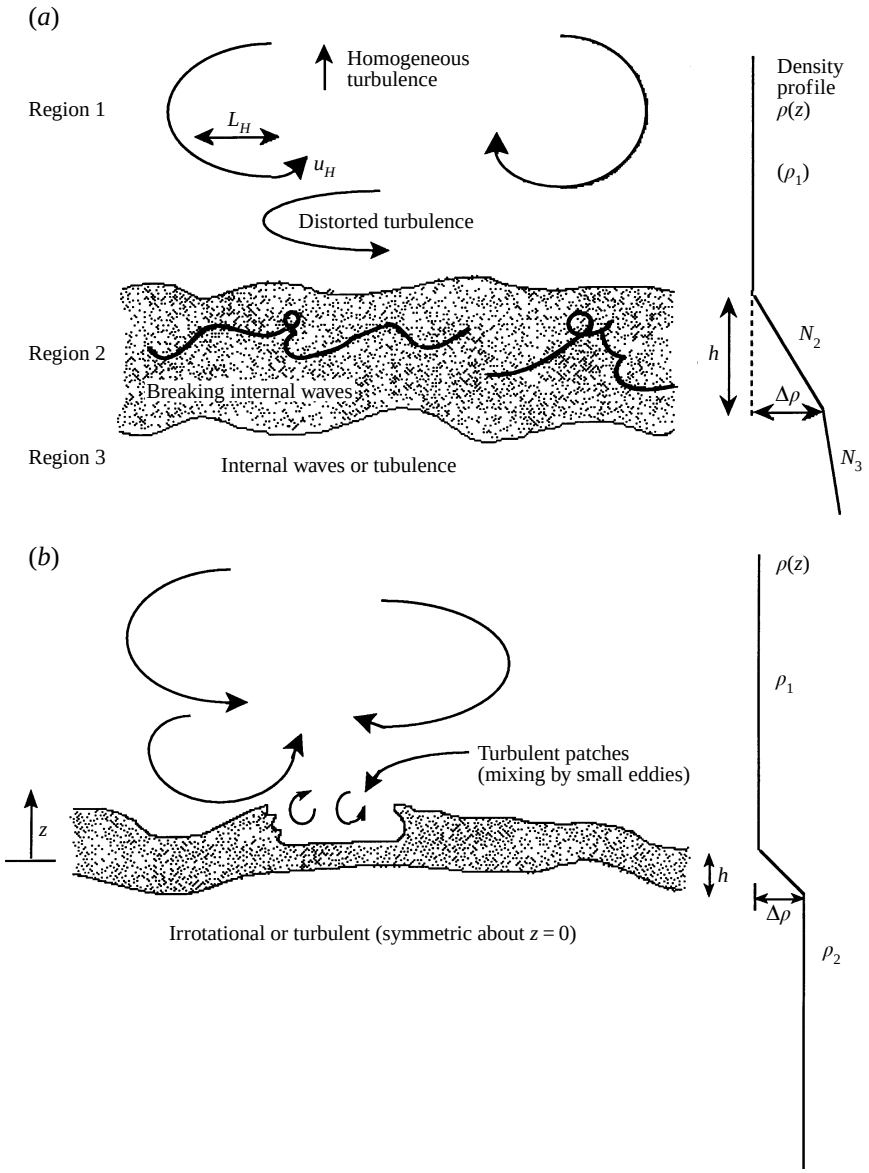

FIGURE 1. (*a*) A schematic diagram of the three-layer stratification under consideration. Here the intermediate region (2) is of finite thickness and permits the sustaining of different modes of internal waves. (*b*) A special case of (*a*) where the interfacial thickness is small and the interface exhibits the first mode of internal waves.

there are significant internal motions within region 2 which are generally dissipative (i.e. modes 2, 3, ...). Specifying these different forms of interfacial motions provides a useful classification for different experiments and models based on Ri, $Ri_{(I)}$ and $Ri_{(3)} = N_3^2 L_H^2 / u_H^2$, where N_3 is the buoyancy frequency of region 3; see table 1.

Dimensional arguments and the preceding discussion suggest that the motion field in a general situation having the configuration of figure 1(*a*) should depend on the three Richardson numbers $Ri, Ri_{(I)}$ and $Ri_{(3)}$ (too often, different situations are compared and, not surprisingly, different results are obtained). Table 1 shows that

Case	Motions in different regions: Region 1	Region 3	Richardson numbers: Interface: External Ri	Interface: Internal $Ri_{(I)}$	Stratified region $Ri_{(3)}$	Examples
A	$\mathscr{T}$	I	$\geqslant 1$	$\leqslant \pi^2$	0	Turner (1968); Hannoun & List (1988); Fernando & Long (1985); E & Hopfinger (1986); Nokes (1988) Fleury *et al.* (1991) McGrath *et al.* (1997)
B	$\mathscr{T}$	$\mathscr{W}$	(*a*) 0 (*b*) ~ 1	0 ~ 1	~ 1 $\leqslant 1$	(*a*) Carruthers & Hunt (1986) (*b*) Linden (1975)
C	$\mathscr{T}$	$\mathscr{W}$	(*a*) $\geqslant 1$ (*b*) $\geqslant 1$	$\leqslant \pi^2$ $\geqslant \pi^2$ (*a*) and (*b*)	$\geqslant 1$ $\geqslant 1$	(*a*) Caughey *et al.* (1982) (*b*) Deardorff (1980) Carruthers & Hunt (1997)
D	$\mathscr{T}$	$\mathscr{T}$	$\geqslant 1$	$\leqslant \pi^2$	0	Turner (1968) Fernando (1995) McGrath *et al.* (1997)

TABLE 1. Studies of turbulent and stratified interfaces.

most previous studies, including a part of the present study, have focused on situation A where the turbulence is on one side only, and the only stratification is within the interface, i.e.

$$u_{(1)} = \mathscr{T}, \quad u_{(3)} = I,$$
$$Ri = \Delta b L_H / u_H^2 \geqslant 1,$$
$$Ri_{(I)} = N_2^2 h^2 / u_H^2 \leqslant \pi^2 \text{ (mode 1)}.$$

In flow type B only region 3 is stably stratified and the density difference across the thin interface is small or negligible. Internal wave motion is generated in region 3 (Carruthers & Hunt 1986),

$$u_{(1)} = \mathscr{T}, \quad u_{(3)} = \mathscr{W}, \quad h/L_H \to 0, \quad Ri \to 0,$$

and

$$Ri_{(3)} = N_3^2 L_H^2 / u_H^2 \leqslant 1.$$

In situation C the interfacial layer may be strongly stratified so that internal wave modes (2, 3, ...) can occur, and region 3 is either weakly stratified or unstratified. This situation corresponds to the analysis of Carruthers & Hunt (1997) and several

computational studies with large-eddy simulations (e.g. Carruthers & Moeng 1987). Here

$$u_{(1)} = \mathscr{T}, \quad u_{(3)} = \mathscr{W}$$
$$Ri_{(I)} \leqslant \pi^2 \text{ (mode 1)}, \quad \text{or} \quad Ri_{(I)} \geqslant \pi^2 \text{ (modes 2, 3, \ldots)},$$
$$Ri_{(3)} \geqslant 1 \quad \text{and} \quad Ri \geqslant 1.$$

In the fourth situation, D, there is significant turbulence in both regions but a strongly stratified layer is located between them. Here

$$u_{(1)} = \mathscr{T}, \quad u_{(3)} = \mathscr{T}, \quad Ri \geqslant 1 \quad \text{and} \quad Ri_{(I)} \leqslant \pi^2.$$

The overall effects of stratification–turbulence interaction on the flow and other phenomena in regions 1 and 2 are that they determine either the rate at which the interface moves, $E_b = \mathrm{d}D/\mathrm{d}t$ (where D is the thickness of the turbulent layer) as in case A; or the average flux of buoyancy across a fixed interface F_b normalized by the mean buoyancy jump (Δb) across the interface, $E_f = F_b/\Delta b$, as in case D (Turner 1986). Both these quantities are called entrainment velocities, but their magnitudes can be generally different as we will show in the subsequent analysis (§ 5.2).

Not surprisingly there is considerable disagreement between experimentally determined magnitudes of E_b/u_H and E_f/u_H as a function of Ri, probably because they depend on the details of the flow structure, which we now review. For all the cases with stably stratified interfaces where $Ri \geqslant 1$, the movement of the interface or the existence of a finite flux across the interface is only possible if the density of fluid elements changes by the action of small-scale turbulence and ultimately by molecular diffusion (a precise statement in this context can be developed following Pearson, Puttock & Hunt 1983). Once the mixing is defined, E_b and E_f can be calculated. A number of different mechanisms and quantitative models have been proposed for these mixing processes at interfaces for $Ri \geqslant 1$. These mechanisms are as follows.

(i) The eddies impact on a thin interface and, as they rebound, generate thin jets of fluid directed from the interface towards the turbulent region. These cause high local gradients between different fluid elements and promote molecular mixing (e.g. Linden 1973).

(ii) The small-scale eddies in region 1 directly generate Kelvin–Helmholtz instabilities across region 2, in which velocity shear leads to overturning billows that break down into small-scale turbulence (e.g. Fleury *et al.* 1991; Mory 1991).

(iii) Turbulent eddies excite wave motion which grows until it becomes nonlinear. In cases A, D and sometimes in C, where the interface is relatively thin ($Ri_{(I)} \leqslant \pi^2$), the interface can flap (mode 1). Laboratory experiments of Hannoun & List (1988) show how these waves break and cause intermittent mixing. Flow visualization studies of McGrath, Fernando & Hunt (1997) show that breaking waves appear as steep fronts on the interface. In case C, where the interface may be thicker ($Ri_{(I)} \geqslant \pi^2$), large-eddy simulation (Carruthers & Moeng 1987) and a theoretical model (Carruthers & Hunt 1997) show that internal waves within the interface can grow until they overturn.

For the 'thin-interface' cases of A and D, all of the above mechanisms can occur simultaneously. Mory (1991) argued (without detailed analysis) that (ii) is dominant and that (iii) has only a small effect. But we argue in this paper via analysis and using the detailed flow field diagnostics of Hannoun, Fernando & List (1988) and Hannoun & List (1988) that mechanism (iii) is dominant, and that, although mechanism (ii) exists, it is less important. We agree with Mory (1991) that mechanism (ii) is relevant

for smaller scales. Further new visualization studies on interfacial mixing are presented in the companion paper by McGrath *et al.* (1997).

In this paper, a linear model is constructed for the distortion of turbulence near the interface and the distorted turbulence field is matched with the waves on the interface. A two-fluid system with a buoyancy (density) jump Δb ($\Delta\rho$) across a thin interfacial layer of thickness h is considered; see figure 1(*b*). The distance z is measured from the centre of the interface. Two configurations are considered, namely (i) an upper turbulent layer ($z > h/2$) and a lower non-turbulent layer ($z < -h/2$) with irrotational fluctuations (case A), and (ii) both upper and lower layers are turbulent (case D).

The method of analysis is similar to that of Carruthers & Hunt (1986), where a shear-free turbulent flow near a density interface is assumed to be similar to that which occurs when a horizontal density interface is inserted into a homogeneous turbulent flow. The undistorted homogeneous turbulence is specified *a priori* using the four-dimensional joint wavenumber/frequency spectra, and the distortions introduced by the insertion of the interface are considered to be irrotational. The resulting flow field outside the interface is the sum of the homogeneous turbulence field and the distorted field. The wave field that can be sustained in the interface, excited by the 'distorted' turbulence near the interface, can then be calculated by proper matching at the boundary between turbulent and interfacial regions. It will be shown that the interface can sustain high-frequency internal waves, but the low-frequency waves break resonantly. The energy absorbed into the interface is then calculated by assuming that the interfacial motion field is maintained in a quasi-stationary state via the energy supplied by the turbulence and the dissipation and buoyancy flux associated with the resonantly breaking low-frequency waves. The entrainment velocities are calculated by considering detailed energetics at the interface.

The paper is arranged as follows. In § 2, the form of the joint wavenumber-frequency energy spectrum of the undistorted homogeneous turbulence is considered. This is an essential input to the model because it is the unsteady motion of different eddy scales that drives the waves on the interface (Hunt & Carruthers 1990). Section 3 is devoted to the development of the model and to the comparison between model predictions of various turbulent quantities and previously published experimental results. The unsteady model is developed in § 4 and the entrainment calculations are given in § 5. Some aspects of shear-free turbulence near highly stable interfaces ($Ri \to \infty$) are discussed in § 6. The paper closes with a summary and discussion in § 7.

Although the measurements of Hannoun *et al.* (1988), Hannoun & List (1988) and Fleury *et al.* (1991) provide a comprehensive set of data for the single-sided stirring case A, no such extensive data exist for the double-sided stirring case D. An experimental programme was carried out simultaneously with the theoretical developments described in this paper, and the results of this investigation are described in the companion paper, McGrath *et al.* (1997).

2. Modelling of homogeneous turbulence

Since the waves in the stratified layer (region 2) are forced by the unsteady eddying motions of region 1, a linear rapid distortion theory (RDT) approach requires modelling the joint wave number ($\boldsymbol{k}$) frequency (ω) spectra of homogeneous turbulence $\chi_{ij}^{H}(\boldsymbol{k}, \omega)$, which is to be distorted by the introduction of the density interface (Hunt & Carruthers 1990). To this end, Carruthers & Hunt (1986) assumed that the main cause of time variation of velocity at a given point in a frame of reference moving with the mean flow is the random advection of fluid elements by the energy-containing eddies

with velocity and length scales u_H and L_H, respectively. The parameterization based on this analysis is strictly valid only for frequencies $\omega > u_H/L_H$. Following Carruthers & Hunt (1986), we use an approximate form of the small-scale high-frequency spectrum

$$\chi_{ij}^H(\boldsymbol{k},\omega) = \phi_{ij}^H(\boldsymbol{k})\delta(|\omega| - ku_H) \quad \text{for} \quad kL_H \gg 1, \quad \omega L_H/u_H \gg 1, \tag{2.1}^d$$

where $\boldsymbol{k} = |k|$, $\delta()$ is a Dirac delta function,

$$\chi_{ij}^H(\boldsymbol{k},\omega) = \frac{1}{(2\pi)^4}\int_{-\infty}^{+\infty}\int_{-\infty}^{+\infty}\int_{-\infty}^{+\infty}\overline{u_i^H(\boldsymbol{x},t)u_j^H(\boldsymbol{x}+\boldsymbol{r},t+\tau)}\,\mathrm{e}^{\mathrm{i}(\boldsymbol{k}\cdot\boldsymbol{r}-\omega\tau)}\mathrm{d}\boldsymbol{r}\,\mathrm{d}\tau \tag{2.2}^d$$

and

$$\phi_{ij}^H(\boldsymbol{k}) = \frac{1}{(2\pi)^3}\int_{-\infty}^{+\infty}\int_{-\infty}^{+\infty}\int_{-\infty}^{+\infty}\overline{u_i^H(\boldsymbol{x},t)u_j^H(\boldsymbol{x}+\boldsymbol{r},t)}\,\mathrm{e}^{-\mathrm{i}(\boldsymbol{k}\cdot\boldsymbol{r})}\mathrm{d}\boldsymbol{r} \tag{2.3}^d$$

is the energy spectrum tensor. Also, $\boldsymbol{k} = (k_1, k_2 k_3)$, $\boldsymbol{x} = (x, y, z)$ is the position, t is the time, r and τ are spatial and temporal separations, respectively, and u_i^H is the instantaneous velocity that can be represented using its random Fourier amplitude S_i^H as

$$u_i^H(\boldsymbol{x},t) = \int_{-\infty}^{+\infty}\int_{-\infty}^{+\infty}\int_{-\infty}^{+\infty}\int_{-\infty}^{+\infty}S_i^H(\boldsymbol{k},\omega)\,\mathrm{e}^{\mathrm{i}(\boldsymbol{k}\cdot\boldsymbol{x}-\omega t)}\mathrm{d}\boldsymbol{k}\,\mathrm{d}\omega. \tag{2.4}^d$$

Note that all the dimensional equations are represented by the superscript ^{d} appearing after the equation number and the overbar denotes averaged quantities. Because the turbulence is homogeneous and stationary, it follows that

$$\overline{S_i^{H\ddagger}(k_1,k_2,k_3,\omega)S_j^H(k_1,k_2,k_3',\omega)} = \chi_{ij}^H(k_1,k_2,k_3',\omega)\delta(k_3 - k_3'), \tag{2.5}^d$$

where ‡ denotes the complex conjugate. A better model of $\chi_{ij}^H(\boldsymbol{k},\omega)$ should allow for the random advection of small eddies by different scales of large eddies; see Chase (1970). However, the use of the simple form (2.1) for $\chi_{ij}^H(\boldsymbol{k},\omega)$ greatly simplifies the calculations, without introducing errors in the distorted spectrum greater than about 10% (Carruthers & Hunt 1997). Thus, throughout the paper we use the form (2.1) to model the high-frequency spectra.

The energy spectrum tensor for isotropic turbulence can be written as

$$\phi_{ij}^H(\boldsymbol{k}) = \frac{E(k)}{4\pi k^4}(k^2\delta_{ij} - k_i k_j), \tag{2.6}$$

where $E(k)$ is the energy spectrum function. Using the von Kármán form for $E(k)$ (Hunt 1973), which is commonly observed in laboratory and geophysical flows, (2.6) can be written as

$$\phi_{ij}^H(\boldsymbol{k}) = g_3\frac{k^2\delta_{ij} - k_i k_j}{(g_2 + k^2)^{17/6}}, \tag{2.7}$$

where $g_2 = \pi\Gamma^2(\frac{5}{6})/\Gamma^2(\frac{1}{3}) = 0.558$, $g_1 = g_2^{5/6}/\pi = 0.1955$ and $g_3 = 55g_1/36\pi = 0.0951$. Note that (2.6) and (2.7) have been non-dimensionalized using $kL_H \to k$, $\omega L_H/u_H \to \omega$ and $\phi_{ij}^H(\boldsymbol{k})/(u_H^2 L_H^3) \to \phi_{ij}^H(\boldsymbol{k})$.

The validity of (2.1) and (2.7) can be tested by comparing the calculations of the Eulerian frequency spectra $\psi_{ij}^H(\omega)$, defined by

$$\psi_{ij}^H(\omega) = \frac{1}{2\pi}\int_{-\infty}^{+\infty}\overline{u_i^H(\boldsymbol{x},t)u_j^H(\boldsymbol{x},t+\tau)}\,\mathrm{e}^{-\mathrm{i}\omega\tau}\mathrm{d}\tau, \tag{2.8}^d$$

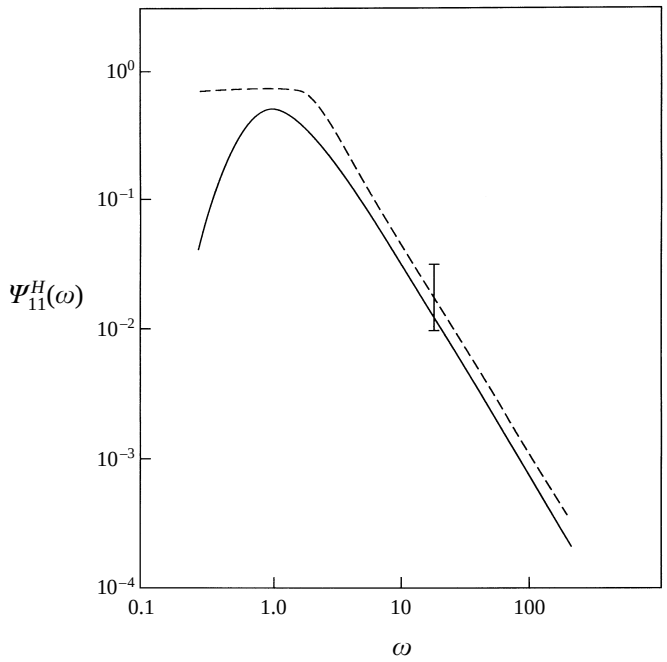

FIGURE 2. Calculated non-dimensional Eulerian frequency spectra (——) and comparison with the measured spectra (- - - -) of Hannoun (1987). Several spectra measured during these experiments were averaged and the mean is shown.

namely

$$\psi_{ii}^H(\omega) = \int_{-\infty}^{+\infty}\int_{-\infty}^{+\infty}\int_{-\infty}^{+\infty} \phi_{ii}(\boldsymbol{k})\delta(|\omega| - k)\mathrm{d}\boldsymbol{k} = \frac{8\pi g_3}{3}\frac{\omega^4}{(g_2+\omega^2)^{17/6}}, \tag{2.9}$$

for $i = 1$, 2 or 3. At large ω, (2.9) is consistent with the Eulerian frequency spectra proposed by Tennekes (1975):

$$\psi_{ii}^H(\omega) = C\varepsilon^{2/3}u_H^{2/3}\omega^{-5/3}, \tag{2.10}^d$$

where the turbulent kinetic energy (TKE) dissipation rate ε has been parameterized using $\varepsilon = C_1 u_H^3/L_H$ and $C = 8\pi g_3/3C_1^{2/3}$. As mentioned, the above model is not accurate for low frequencies of the spectrum.

Since our model predictions will be compared in detail with the measurements of laboratory oscillating-grid mixing-box experiments, it is appropriate to compare the experimental turbulence to the theoretical ideas of homogeneous turbulence assumed in the model. When the turbulence is induced by an oscillating grid, the energy-flux divergence (representing nonlinear processes) in the TKE equation is the predominant energy transport term, and it is associated with greater mixing and straining of eddies than in the case of uniform flow past a grid. Even at relatively low Reynolds numbers ($Re = u_H L_H/\nu$, where ν is the kinematic viscosity) of the order of 100, the resulting turbulence produces a well-defined $\omega^{-5/3}$ range.

A comparison of (2.9) with the oscillating-grid experimental results of Hannoun (1987) is shown in figure 2. The spectral slope at large ω is in agreement with (2.9), but the experimental value of g_3 (≈ 0.18) is clearly higher than the cannonical empirical value of 0.0951. In what follows, however, the standard (von Kármán spectrum)

value of g_3 is used; in some cases the effect of g_3 on the model results will also be evaluated. It is also interesting to note that the coefficient C in (2.10) is estimated as $C \approx 1.1$, using the value of $C_1 \approx 0.61$ extracted from Hopfinger & Toly (1976) and $g_3 = 0.0951$. (Hopfinger & Toly presented data on the Taylor microscale λ and the Reynolds number Re; using $\lambda/L_H = (15/C_1)^{1/2} Re^{-1/2}$, the above value of C_1 was evaluated. Apparently this value of C_1 was found earlier by Bouvard & Dumas (1967)). Calculations based on the analysis of Chase (1970), kinematic simulations of Fung *et al.* (1992) and recent experiments of Kit, Fernando & Brown (1995) give $C \approx 0.8 \pm 0.1$.

3. A stationary model for wave–turbulence interactions at thin interfaces

3.1. *Formulation of the problem*

In our analysis of the flow, shown schematically in figure 1(*b*), the following physically based assumptions are used by close inspection of previous laboratory experiments dealing with both time and space variation of the interfacial-layer boundaries adjacent to turbulent flows.

(i) The density profile within the interface is linear so that its buoyancy frequency is given by $N_2^2 = \Delta b/h$. Outside the interface, i.e. when $|z| > h$, the stratification is zero. These assumptions are supported by the experimental work of Crapper & Linden (1974) and Fernando & Long (1985).

(ii) h is sufficiently small so that the internal Richardson number satisfies

$$Ri_{(I)} = N_2^2 h^2/u_H^2 \ll Ri_{(I)}^c, \tag{3.1a}$$

where $Ri_{(I)}^c$ is a critical value, but N_2 and L_H are sufficiently large so that the external Richardson number is large,

$$Ri = \Delta b L_H/u_H^2 \gg 1. \tag{3.1b}$$

As will be discussed below, the criterion (3.1*a*) is necessary for the interface to be dominated by the first mode of internal waves. The external Richardson number criterion (3.1*b*) ensures that the buoyancy forces at the interface are sufficiently strong so that turbulent eddies do not break it up without allowing internal waves to develop within the interface. The model of Carruthers & Hunt (1997) shows that $Ri_{(I)}^c = \pi^2$ and the observations described in McGrath *et al.* (1997) indicate that the interfacial mixing is dominated by internal wave breaking when $Ri > 30$ or so.

(iii) Assuming that (in an Eulerian frame) the turbulence and wave motions are statistically stationary processes and homogeneous in the horizontal plane, the vertical velocity fluctuation w can be expressed as a Fourier transform in horizontal wavenumbers and frequency as

$$w(x, y, z, t) = \int_{-\infty}^{+\infty} \int_{-\infty}^{+\infty} \int_{-\infty}^{+\infty} \hat{w}(k_1, k_2, z, \omega) \mathrm{e}^{\mathrm{i}(k_1 x + k_2 y - \omega t)} \mathrm{d}k_1 \mathrm{d}k_2 \mathrm{d}\omega \tag{3.2}^d$$

(a similar expression can be written for other velocity components and the pressure). The linear internal-wave equations(Phillips 1977; Gill 1982) based on the momentum, continuity and density conservation equations within the interface can be written as

$$\frac{\partial^2}{\partial t^2}(\nabla^2 w) + N^2(\nabla_h^2 w) = 0 \tag{3.3}^d$$

and

$$\frac{\partial^2 w}{\partial t^2} + N^2 w = -\frac{1}{\rho_0}\frac{\partial^2 p}{\partial z \partial t}, \tag{3.4}^d$$

where p is the pressure perturbation and $\nabla_h^2 = \partial/\partial x^2 + \partial/\partial y^2$.
Using (3.2), the equation for $\hat{w}$ in the interfacial layer (region 2) can be written as

$$\frac{\mathrm{d}^2\hat{w}}{\mathrm{d}z^2} + \frac{(N^2-\omega^2)}{\omega^2}k_{12}^2\hat{w} = 0, \tag{3.5a}^d$$

where $k_{12}^2 = k_1^2 + k_2^2$. The non-dimensional form of (3.5) becomes

$$\frac{\mathrm{d}^2\hat{w}}{\mathrm{d}z^2} + Ri\left[1 - \frac{\omega^2}{Ri_{(I)}}\left(\frac{h}{L_H}\right)^2\right]\frac{k_{12}^2\hat{w}}{\omega^2} = 0, \tag{3.5b}$$

which implies that when the interface is dominated by sufficiently long waves, $\hat{w}$ may vary linearly across the layer and the higher modes of internal waves are not excited in the interface. Thus, it is possible to write

$$\hat{w}(z=-h/2) = \hat{w}(z=h/2) - \lambda h, \tag{3.6a}^d$$

where for consistency with the outer flow $\lambda \sim u_H/L_H$. If $h < L_H$, it is possible to recover the usual kinematic boundary condition for the first mode of internal waves on the interface,

$$\hat{w}(z=-h/2) = \hat{w}(z=h/2). \tag{3.6b}$$

As mentioned, the detailed model presented by Carruthers & Hunt (1997) shows that the conditions for (3.6*b*) to be valid exist when $N_2^2h^2/u_H^2 < \pi^2$. Thus, it is possible to estimate the range of h/L_H necessary to satisfy (3.6*b*) as $h/L_H \leqslant \pi^2 Ri^{-1}$. Given that the interface is dominated by the internal waves when $Ri > 30$ or so, this requirement becomes $h/L_H \leqslant 0.3$. Laboratory experiments of Perera, Fernando & Boyer (1994), however, have indicated that $Ri_{(I)} < \pi^2$ may not be the criterion for the sustenance of the first mode. They observed the first mode up to $Ri_I \approx 50$ or so, according to which the requirement for the first mode of waves is $h/L_H \leqslant 1.6$. The bulk of the oscillating-grid mixing-box experiments reported thus far appear to have yielded h/L_H values conducive to the generation of the first mode of internal waves. Figure 3 (*a*, *b*) shows the boundaries of density interfaces corresponding to previous oscillating-grid experiments. Note the approximate in-phase oscillations of different density contours, characteristic of the flapping mode. These observations are also corroborated by the results of McGrath *et al.* (1997).

(iv) Integration of (3.5) across the interface yields (Phillips 1977)

$$\left(\frac{\mathrm{d}\hat{w}}{\mathrm{d}z}\right)_{z=h/2} - \left(\frac{\mathrm{d}\hat{w}}{\mathrm{d}z}\right)_{z=-h/2} = -\frac{\Delta b}{\omega^2}k_{12}^2\hat{w}(0), \tag{3.7}^d$$

which provides an additional (dynamical) boundary condition for the interface.

(v) Over a low-frequency range (say $\omega < \omega_c$), the waves are nonlinear; they are primarily driven by and do not react back on interfacial motions in the linear high-frequency range. For a physical description of these motions, see McGrath *et al.* (1997). The calculation of ω_c is given in § 3.3.2 (*c*).

(vi) Atmospheric observations of Caughey & Palmer (1979) and the laboratory measurements of Kit, Strang & Fernando (1997) indicate that in the turbulent region, above the interface over a distance of the order L_H, the dissipation rate of TKE per unit mass (ε) is approximately constant. It follows that $\mathrm{d}\bar{\Omega}^2/\mathrm{d}z \approx 0$, where Ω is the

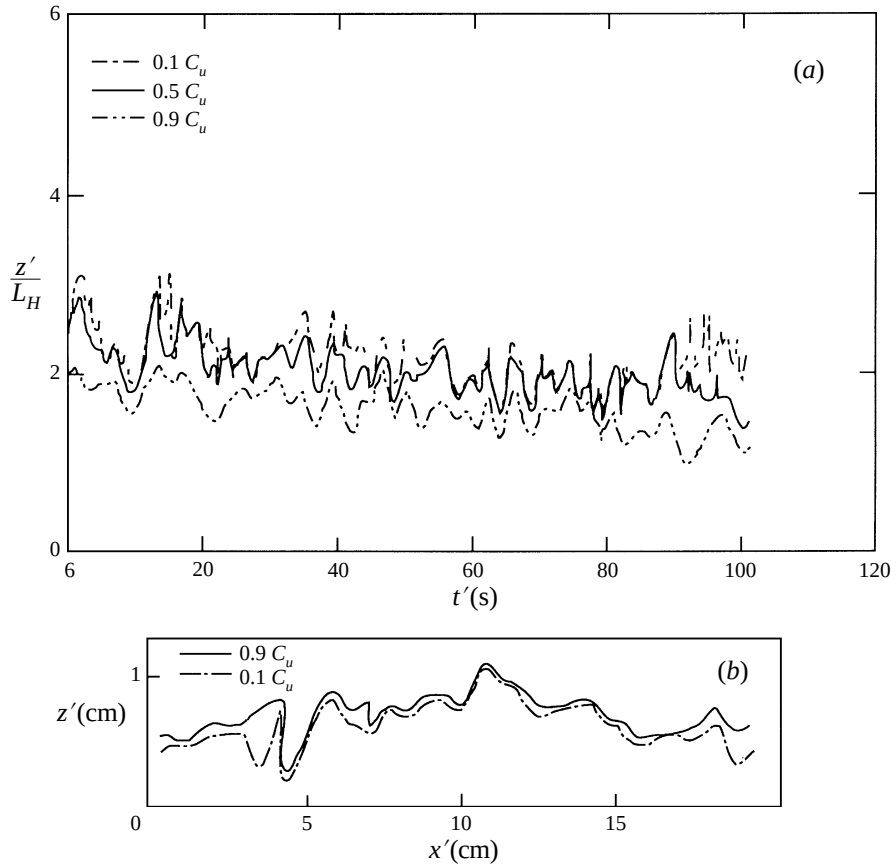

FIGURE 3. (*a*) Variation of the boundaries of the interface with time t' at a given vertical section, from Hannoun & List (1988). In the experiments, the upper turbulent layer was dyed with a concentration C_u and the contours of constant concentration are shown. The Richardson number for this run is $Ri = \Delta b L_H / u_H^2 = 24$. (*b*) Spatial ($x'$) variation of bounding concentration contours of the interface, taken at a given time, from Redondo (1990). The height z', horizontal distance x' and time t' have arbitrary origins.

fluctuation of vorticity. Large-eddy simulation results of Moeng (1986) are consistent with this deduction. As pointed out by Hunt (1984), this implies that the distorted turbulent velocity field $\boldsymbol{u}(x,t)$ near the interface can be approximated as the sum of the homogeneous velocity field $\boldsymbol{u}^H$ and an irrotational velocity field $\boldsymbol{u}^D(x,t)$, namely

$$\boldsymbol{u}(\boldsymbol{x},t) = \boldsymbol{u}^H(\boldsymbol{x},t) + \boldsymbol{u}^D(\boldsymbol{x},t), \tag{3.8}^d$$

where $\boldsymbol{u}^D(\boldsymbol{x},t) = -\nabla\varphi$ and φ is a velocity potential that satisfies

$$\nabla^2\varphi = 0. \tag{3.9}^d$$

The Fourier transforms of $u_i, \hat{u}_i$ (as in (3.2)) may be expressed in terms of a four-dimensional Fourier transform of the homogeneous turbulence $S_i^H(\boldsymbol{k},\omega)$ (defined in (2.4)) and a transfer function $M_{in}(\boldsymbol{k},\omega;z)$ as

$$\hat{u}_i(k_1,k_2,\omega,z) = \int_{-\infty}^{+\infty} M_{in}(\boldsymbol{k},\omega;z) S_n^H(k_1,k_2,\omega,z)\mathrm{d}k_3. \tag{3.10}^d$$

(vii) It is assumed that when the turbulence is present above and below the interface, the undistorted turbulent velocity fields in the layers are both homogenous and stationary, but uncorrelated.

3.2. *Solution procedure*

3.2.1. *Case 1: turbulence in the upper layer only* (*single-sided stirring*)

In this case, the lower layer consists of irrotational fluctuations described by (3.9). Seeking solutions of the form

$$\varphi(x,y,z,t)=\int_{-\infty}^{+\infty}\int_{-\infty}^{+\infty}\int_{-\infty}^{+\infty}\hat{\varphi}(k_1,k_2,\omega,z)\mathrm{e}^{\mathrm{i}(k_1x+k_2y-\omega t)}\mathrm{d}k_1\mathrm{d}k_2\mathrm{d}\omega, \tag{3.11}^d$$

and since φ is bounded as $z\to\pm\infty$, it is possible to evaluate $\varphi(\boldsymbol{x},t)$ for upper and lower layers separately, and thence the velocity fields. Comparison of these with (3.2) gives

$$\hat{w}(k_1,k_2,\omega,z)=\int_{-\infty}^{+\infty}S_3^H\mathrm{e}^{\mathrm{i}k_3z}\mathrm{d}k_3+Bk_{12}\mathrm{e}^{-k_{12}z}, \tag{3.12a}^d$$

$$\hat{u}_i(k_1,k_2,\omega,z)=\int_{-\infty}^{+\infty}S_i^H\mathrm{e}^{\mathrm{i}k_3z}\mathrm{d}k_3-\mathrm{i}k_iB\mathrm{e}^{-k_{12}z}\quad(\mathrm{i}=1,2), \tag{3.12b}^d$$

for the upper turbulent layer, and

$$\hat{w}(k_1,k_2,\omega,z)=-Ak_{12}\mathrm{e}^{k_{12}z}, \tag{3.13a}^d$$

$$\hat{u}(k_1,k_2,\omega,z)=-\mathrm{i}Ak_i\mathrm{e}^{k_{12}z} \tag{3.13b}^d$$

for the lower layer, respectively, where A and B are determined using the interfacial conditions (3.6*b*) and (3.7):

$$A=\frac{\displaystyle\int_{-\infty}^{+\infty}(k_{12}+\mathrm{i}k_3)S_3^H\mathrm{d}k_3}{k_{12}^2(2-\Delta bk_{12}/\omega^2)};\quad B=\frac{\displaystyle\int_{-\infty}^{+\infty}(\mathrm{i}k_3+\Delta bk_{12}^2/\omega^2-k_{12})S_3^H\mathrm{d}k_3}{k_{12}^2(2-\Delta bk_{12}/\omega^2)}. \tag{3.14}^d$$

There are no valid steady solutions to the linear equations for $\omega=\omega_1=(\Delta bk_{12}/2)^{1/2}$. In fact, the unsteady analysis given in § 4 indicates that the interfacial velocity for this case grows with time.

3.2.2. *Case 2: turbulence in both layers* (*double-sided stirring*)

A simple extension of the analysis presented in § 3.2.1 can be used to describe the flow when there is turbulence on both sides of the interface, provided that the assumptions (i)–(vii) of § 3.1 remain valid. Maintenance of interfacial conditions (3.6*b*) and (3.7) requires that the distortion field $u^D(\boldsymbol{x},t)$ should be different from that of the single-sided case.

The solution procedure here is similar to that given in § 3.2.1. It is, however, necessary to define $S_{3(+)}^H$ and $S_{3(-)}^H$ for the turbulence above and below the interface, and the coefficients corresponding to A and B in (3.12) and (3.13) can be evaluated using (3.2) and (3.12*a*, *b*). For example, we obtain

$$B=\left(\frac{\displaystyle\int_{-\infty}^{+\infty}S_{3(+)}^H\left(\mathrm{i}k_3+\frac{\Delta bk_{12}^2}{\omega^2}-k_{12}\right)\mathrm{d}k_3}{k_{12}^2(2-\Delta bk_{12}/\omega^2)}\right)-\left(\frac{\displaystyle\int_{-\infty}^{+\infty}S_{3(-)}^H(\mathrm{i}k_3-k_{12})\mathrm{d}k_3}{k_{12}^2(2-\Delta bk_{12}/\omega^2)}\right). \tag{3.15}^d$$

The solution for the lower layer also takes the form of (3.12*a*, *b*) with $e^{-k_{12}z}$ replaced by $e^{k_{12}z}$. It is again noted that these solutions are not valid for $\omega = (\Delta b k_{12}/2)^{1/2}$. From assumption (vii), it follows that $\overline{S^H_{3(+)} S^H_{3(-)}} = 0$.

3.3. *Calculation of the energy spectra*

3.3.1. *Linear theory*

From (3.10) and (2.5), the joint horizontal wavenumber–frequency spectra of the distorted turbulence defined by

$$\Xi_{ij}(k_1, k_2, \omega, z) = \frac{1}{(2\pi)^3} \times \int_{-\infty}^{+\infty} \int_{-\infty}^{+\infty} \int_{-\infty}^{+\infty} \overline{u_i(x, y, z, t) u_j(x+r_x, y+r_y, z, t+\tau)}\, e^{i(k_1 r_x + k_2 r_y - \omega\tau)} dr_x dr_y d\tau \qquad (3.16)$$

can be evaluated as

$$\Xi_{ij}(k_1, k_2, \omega, z = 0) = \int_{-\infty}^{+\infty} M^{\ddagger}_{il} M_{jn} \chi^H_{ln} dk_3. \qquad (3.17)$$

The transfer function M_{ij} follows from (3.12*a*, *b*) and (3.14). Then, by using (3.17) and after some manipulation, the non-dimensional spectra for the vertical velocity component at the interface $z = 0$ can be written as

$$\Xi_{ij}(k_1, k_2, \omega, z = 0) = \int_{-\infty}^{+\infty} \frac{1 + (k_3/k_{12})^2}{(2 - Rik_{12}/\omega^2)^2} \chi^H_{33}(\boldsymbol{k}, \omega) dk_3, \qquad (3.18)$$

for the single-sided stirring case. For the double-sided stirring case, if the turbulence above and below the interface has the same statistics,

$$\Xi_{ij}(k_1, k_2, \omega, z = 0) = \int_{-\infty}^{+\infty} \frac{2[1 + (k_3/k_{12})^2]}{(2 - Rik_{12}/\omega^2)^2} \chi^H_{33}(\boldsymbol{k}, \omega) dk_3, \qquad (3.19)$$

where $Ri = \Delta b L_H / u_H^2$ is the external Richardson number based on velocity and length scales of undistorted turbulence. Note that the latter is just twice the former.

In mixing experiments, it is common to measure the one-point Eulerian frequency spectrum $\psi_{33}(\omega, z)$. This can be derived from (3.18) or (3.19), using (2.1) and (2.7) and integrating over k_1, k_2 and k_3. At the interface ($z = 0$)

$$\psi_{33}(\omega, 0) = \frac{\pi g_3 \omega^4}{2(g_2 + \omega^2)^{17/6}} \int_0^{\pi} \frac{\sin\theta}{(1 - \mu \sin\theta)^2} d\theta, \qquad (3.20)$$

for the single-sided stirring case, and twice this value for the double-sided stirring case, where the ratio between the dimensionless maximum resonant frequency ($Ri/2$) and ω is $\mu = Ri/2\omega = \Delta b / 2u_H \omega$. Note that for the high-frequency spectra, where $\mu < 1$ (or when $\omega > \omega_r$, where $\omega_r = \Delta b / 2u_H$), the above integral gives

$$\psi_{33}(\omega, 0) = \frac{\pi g_3 \omega^4}{2(1 - \mu^2)(g_2 + \omega^2)^{17/6}} \left\{ 2 + \frac{\pi\mu}{(1 - \mu^2)^{1/2}} + \frac{2\mu}{(1 - \mu^2)^{1/2}} \tan^{-1} \frac{\mu}{(1 - \mu^2)^{1/2}} \right\}, \qquad (3.21)$$

for the single-sided case and twice this value for the double-sided stirring case.

Measurements of $\psi_{33}(\omega, 0)$ have been made by Fleury *et al.* (1991) for the case of single-sided stirring and a comparison of their data with (3.21) is given in figure 4. These measurements have been obtained using standard mixing-box experiments,

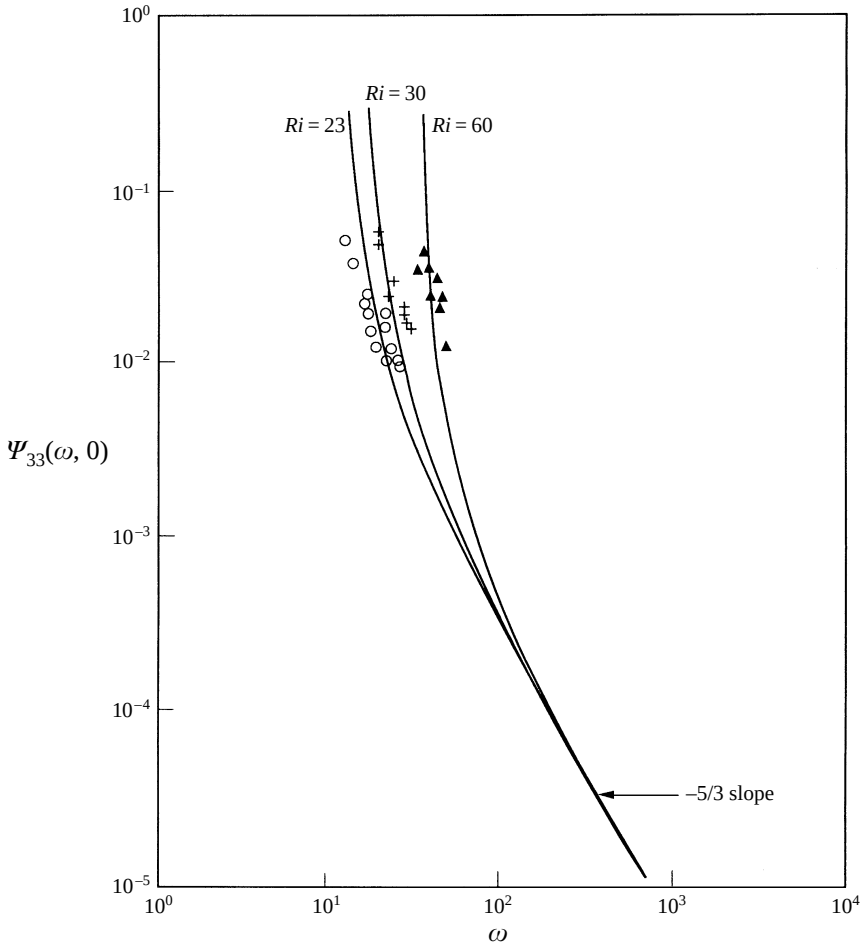

FIGURE 4. A comparison of non-dimensional Eulerian frequency spectra, calculated using (3.21) (solid lines), for different Ri, with the experimental results of Fluery *et al.* (1991): ○, $Ri = 23$; +, $Ri = 30$; ▲, $Ri = 60$. Only the data satisfying $\omega > Ri/2$ are shown. Amplitude spectrum $\psi_{33}^d(\omega)$ data have been converted to energy spectrum data using $\psi_{33}(\omega, 0) = \psi_{33}^d(\omega)/\omega^2$.

wherein a two-fluid system is subjected to agitation by an oscillating grid in the top layer. Although some of their data have been taken in the presence of background rotation, it is expected that the rotation has an insignificant influence on high-frequency motions. Only the data satisfying $\mu < 1$ are shown, and the agreement with (3.21) is good.

3.3.2. *Nonlinear model*

For $\mu > 1$, the integral (3.20) becomes improper, giving unbounded values for $\psi_{33}(\omega, 0)$. These singularities can be interpreted as resonant modes, in which the waves grow to finite amplitudes and break, owing to the build-up of energy within the stratified layer. The steady linear theory described above is not valid for these waves; either a full nonlinear theory is required or a new physical hypothesis must be developed based on observations which enable the low-frequency spectra to be calculated. Considering the complexity and strongly nonlinear nature of the problem

as well as limited capabilities of available mathematical tools to handle such problems, we have resorted to the latter approach.

The proposed nonlinear model is mainly based on previous observations as well as on certain new findings reported in the companion paper by McGrath *et al.* (1997). The essential feature of the model is the use of a mathematical requirement pertinent to the discontinuous nature of the interface as a result of breaking waves (which is an experimental observation). Thus there is a close connection between the knowledge gained by laboratory experiments and development of the model. In what follows the laboratory observations will be first discussed, followed by the development of the nonlinear model.

(*a*) *Laboratory observations*

Laboratory observations indicate that waves on the interface have a wide range of length and time scales and, as they travel randomly over the interface, interact with others and amplify beyond a stable state to break intermittently (Hannoun & List 1988; McGrath *et al.* 1997). Clearly sufficient energy is dissipated to keep the interface in a quasi-stationary state. Observations of these breaking waves show that they generate turbulent patches at the interface and lead to microscale and molecular mixing between the high- and low-density fluids. Partially mixed fluid in these patches, with densities intermediate to those of the upper and lower layers, can be scoured by the turbulent eddies and carried into the turbulent region.

Figure 5(*a–c*) shows snapshots of the entrainment interface, taken by Hannoun *et al.* (1988), which indicate intermittent (spatial) distribution of strong mixing events (marked by X). The events marked by Y are presumably Kelvin–Helmholtz (K–H) instabilities (with regions of vorticity concentration and roll-over) resulting from the sloshing of eddies over the interface. It appears, however, that these K–H events are rare and cause little mixing (especially at moderate and large Ri) compared to breaking of waves. Figure 5(*d*) shows a temporal view of the interface in which the evolution at a single vertical line through the interface is presented; this will be further discussed below.

(*b*) *Mixing mechanisms*

As mentioned in § 1, observations made over a range of external Richardson numbers Ri indicate that the dominant entrainment mechanism depends on Ri. The interfacial wave breaking considered in this paper is predominant in the range $30 < Ri < 100$ (McGrath *et al.* 1997), and several instability mechanisms can be attributed to this mixing mechanism.

A plausible mechanism proposed by Phillips (1977, p. 219) is shown in figure 5(*e*). Accordingly, during the resonant growth of the wave amplitude (a), the internal rate of strain within the wave increases and the local Richardson number Ri_g drops according to

$$Ri_g = \left(\frac{N}{\omega} - \frac{\omega}{N}\right)^2 k^{-2} a^{-2}. \qquad (3.22)^d$$

When the amplitude grows to such a level that Ri_g drops below a critical value, the waves can break internally. An alternative mechanism proposed by Davis & Acrivos (1967) deals with nonlinear interaction between the waves. According to their analysis, when a primary wave of wavenumber k_0 and frequency ω_0 is perturbed by two infinitesimal wave-like disturbances with wavenumbers k_1 and $k_1 + k_0$ and

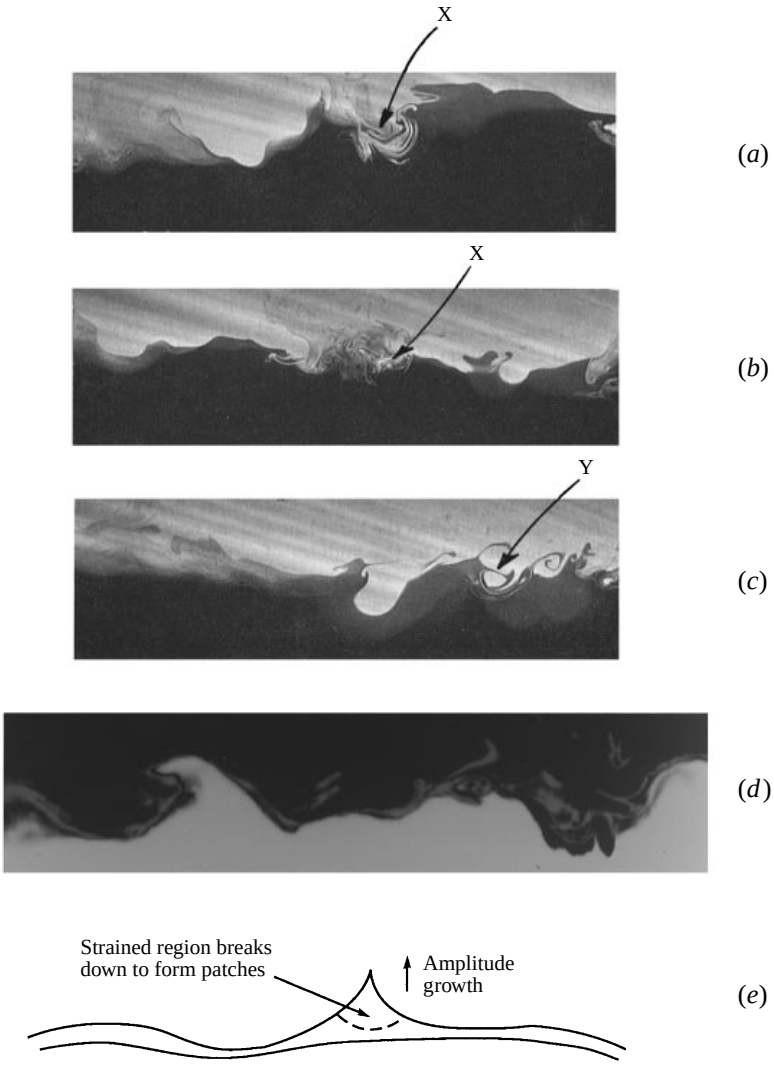

FIGURE 5. (*a–c*) Photographs showing the spatial structure of an entrainment interface, taken from Hannoun *et al.* (1988); $Ri \approx 60$. The patches formed due to wave breaking are depicted by X and possible K–H instabilities due to the eddies sloshing over the interface are marked by Y. (*d*) A time record of interfacial evolution taken at a single vertical line through the interface. The variation of the concentration distribution with time is shown. Different shades indicate different concentrations (from unpublished work of Dr Imad Hannoun). (*e*) A possible mechanism for the breakdown of a growing internal wave into a turbulent patch.

frequencies ω_1 and $\omega_1 + \omega_0$, the disturbances can grow exponentially whence the primary wave amplitude exceeds a certain value. Waves of various wavelengths and frequencies are present in the entrainment interface, and hence may excite such triad-resonant interacting unstable modes, in addition to the forced resonant modes evident from the present analysis. Contributions arising from such nonlinear wave interactions are not explicitly considered here, but the overall effects of low-frequency wave breaking are included in a simple model that will be described next.

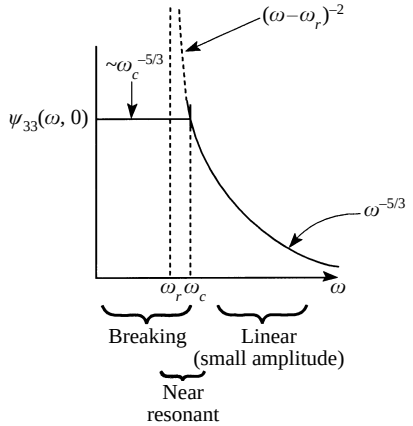

FIGURE 6. A schematic of the frequency (energy) spectrum $\psi_{33}(\omega, 0)$ of the vertical velocity at the interface, derived using the present work. The magnitude or the asymptotic dependence of the spectrum on frequency are indicated on the diagram for different frequency ranges.

(*c*) *Models for displacement and velocity spectra*

In the frequency range $\omega > \omega_r (= \Delta b/2u_H)$, the frequency spectrum of the interfacial vertical velocity is given by (3.21), and for further analysis it is necessary to develop a model for low-frequency velocity statistics over the frequency range where the waves are breaking resonantly. Linear analysis (3.18) shows that the resonant breaking occurs for $\omega < \omega_r$, but certain non-resonant frequencies in the vicinity of ω_r are also expected to have high amplitudes and hence are liable to break. Thus in a frequency subrange $\omega < \omega_c$, where $\omega_c > \omega_r$, breaking internal waves are expected to produce well-separated sharp discontinuities in the displacement of the interface (Figure 5*a–c*). The critical frequency ω_c should be determined by considering the nature of the breaking interface. To this end, we will use the known mathematical result that the one-dimensional wavenumber spectrum of a discontinuous function (for this case, interfacial displacement ζ), with well-separated discontinuities, in the x- or y-direction is proportional to k_1^{-2} or k_2^{-2} (Courant & Hilbert 1953; Moffatt 1984; Hunt *et al.* 1991). Since these waves propagate and/or are advected over the interface, for a fixed observer there are discontinuities in time. Assuming that their speed is only weakly dependent on their amplitude, the frequency spectrum of the vertical displacements can also be written as $\psi^d(\omega) \propto \omega^{-2}$. For weakly nonlinear waves, it is easily shown that the vertical velocity spectrum $\psi_{33}(\omega, 0) \approx \psi^d(\omega)\omega^2$, and therefore for $\omega < \omega_c$

$$\psi_{33}(\omega, 0) \sim \text{ constant.} \qquad (3.23)^d$$

The time traces of wave amplitude shown in figure 5(*d*) indicate discontinuities of the amplitude–time profiles, which is consistent with the vertical velocity spectrum of breaking interfaces having a rather flat region. The frequency spectrum derived from the linear theory and nonlinear model is shown schematically in figure 6 with magnitudes or frequency dependence of different terms. Further experimental evidence for (3.23) is given in McGrath *et al.* (1997).

To illustrate the physical reality of the proposed model, a spectrum of the vertical velocity fluctuations associated with the first mode of internal waves in a thin oceanic thermocline, forced by the mixed-layer turbulence, is shown in figure 7; general similarities can be seen with figure 6, although some deviations are evident. A similar

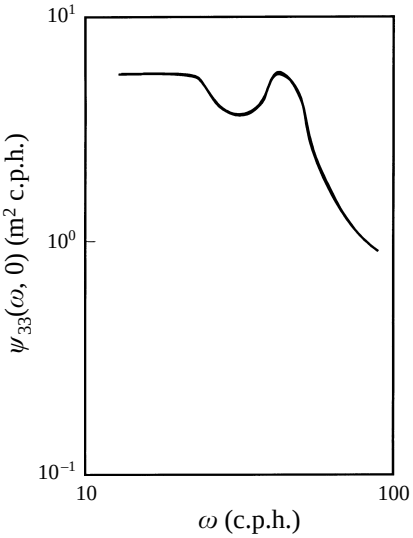

FIGURE 7. Frequency spectrum $\psi_{33}(\omega, 0)$ of vertical velocity fluctuations of the first mode of internal waves, as calculated from the oceanic measurements of Brekhovskikh *et al.* (1975).

trend has been noticed in the spectra measured by Dr Imad Hannoun (personal communication) and in McGrath *et al.* (1997). It is expected that the approximate spectral form proposed here is sufficient to capture the essential features of quasi-stationary solutions. An analogous approach was used by Tennekes & Lumley (1973) for modelling Lagrangian velocity spectra of turbulence.

Therefore, from (3.21) and (3.23), the spectrum for the interfacial vertical velocity has the following form:

$$\psi_{33}(\omega, 0) = \begin{cases} I(\omega) & \text{for} \quad \omega > \omega_c \\ I(\omega_c) & \text{for} \quad \omega > \omega_c, \end{cases} \tag{3.24}^d$$

where $I(\omega)$ is either the right-hand side of (3.21) or twice that value, for single-sided and double-sided stirring, respectively.

The cut-off frequency ω_c (or its dimensionless form $\mu_c = Ri/2\omega_c$) can be estimated using physical arguments, by considering the relative energy of the breaking nonlinear waves and linear forced high-frequency waves. Since the nonlinear waves in the low-frequency range are not directly correlated with turbulence (as explained in § 3.2), the energy of the nonlinear (e_{NL}^2) spectral regime must be derived from the energy (e_L^2) in the forced linear regime residing in the frequency range $\omega > \omega_c$, and must be of the same order. In other words, if $e_{NL}^2 < e_L^2$, nonlinear processes would lead to the growth of e_{NL}^2 because the eigenmodes and other resonant modes would grow. On the other hand, if $e_{NL}^2 > e_L^2$, there would be a rapid energy cascade toward high frequencies until a new equilibrium is set up.

Here, for simplicity, only the energies of the vertical component are considered in estimating ω_c (or μ_c), although a more accurate estimate requires consideration of the total energy. (Large-eddy simulation of Siegel & Domaradzki (1994) has shown that, at a given wavenumber, the vertical component of velocity is a good indicator of the total energy). To this end, it is convenient to define the parameter Γ as

$$\Gamma = \omega_c I(\omega_c) \Big/ \int_{\omega_c}^{\infty} I(\omega) \mathrm{d}\omega, \tag{3.25}^d$$

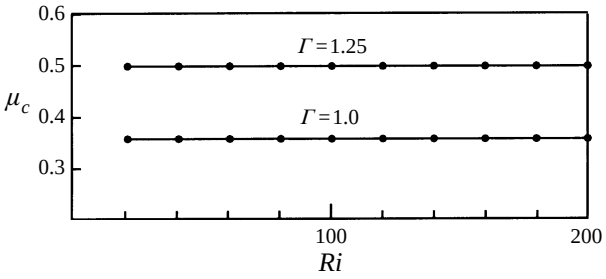

FIGURE 8. The variation of μ_c with the Richardson number *Ri*, for various ratios of (vertical) energies in nonlinear and linear wave regimes Γ.

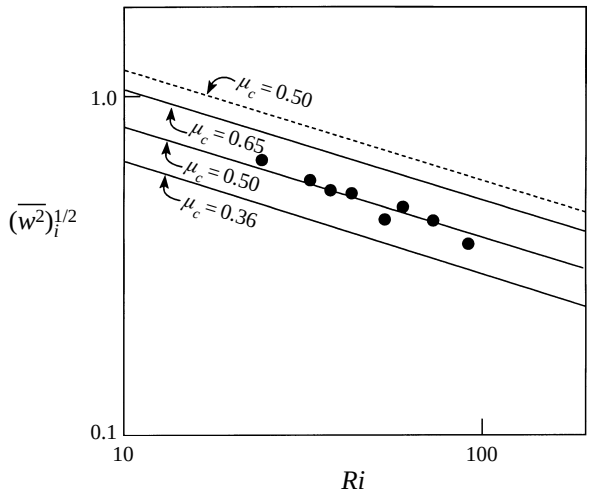

FIGURE 9. Variation of calculated and experimental normalized r.m.s. vertical velocity fluctuation with the Richardson number: ——, calculations for the single-sided stirring case with $\mu_c = 0.36, 0.5$ and 0.65; •, experimental results of Hannoun & List (1988) for single-sided stirring case; - - - -, calculations for double-sided stirring case with $\mu_c = 0.5$.

which signifies the ratio of the contributions from the nonlinear and linear spectral regimes to the vertical velocity. Numerically evaluated μ_c for various Γ and *Ri* of interest are shown in figure 8. For both single- and double-sided cases, $\Gamma = 1.0$ when $\mu_c \approx 0.36$, independent of *Ri*. As will be discussed in § 3.4, the laboratory experimental data for the single-sided case agrees best with the theoretical model predictions when $\mu_c \approx 0.5$, which corresponds to $\Gamma = 1.25$. This argument on the equipartition of energy is consistent with the analysis of a one-dimensional nonlinear forced system by Thompson (1989) who showed, *inter alia*, how the linear forcing dominates when $\omega > \omega_c$ and how chaotic switching between 'eigen' states can occur when $\omega \ll \omega_c$.

3.4. *Interfacial velocity*

Given (3.24), the interfacial velocity $(\overline{w^2})_i$ can be calculated using

$$(\overline{w^2})_i = \int_{-\infty}^{+\infty} \psi_{33}(\omega, 0)\mathrm{d}\omega. \tag{3.26}$$

This integral was evaluated numerically and the results are shown in figure 9. Three solid lines represent, respectively, the calculations for three different spectral cut-offs,

$\mu_c = 0.36$, 0.5 and 0.65, for the single-sided stirring case. Note that the predicted power-law behaviour at large Richardson numbers is independent of the selection of μ_c, namely $(\overline{w^2})_i^{1/2} \propto Ri^{-1/3}$.† As mentioned, the data of Hannoun & List (1988) follow the calculation if $\mu_c = 0.5$ is selected. The double-sided stirring case with $\mu_c = 0.5$ shows a similar power-law behaviour (broken lines), but the actual magnitude of the velocity is larger by a factor of $\sqrt{2}$, as a result of forcing from both sides of the interface.

There are several points to be noted. First, the integral length scale used in Hannoun & List (1988) can be different from the L_H based on the spatial correlation used in the present calculations; they did not measure L_H, but estimated it using the measured integral time scales. The two length scales can be proportional to each other, but their magnitudes may differ. Second, as discussed in § 2, the value of g_3 for oscillating grid turbulence can be higher than the value $g_3 = 0.0951$ based on wind tunnel studies. If $g_3 = 0.18$ (based on Hannoun *et al.'s* 1988 measurements) is used, then the velocity predictions based on $\mu_c = 0.36$ (or $\Gamma = 1$) show a very good match with the data of Hannoun & List (1988). For applications in general geophysical flows, calculations were mainly performed using the standard value of $g_3 = 0.0951$ and with $\mu_c = 0.5$.

3.5. *Interfacial distortions*

The interfacial distortions ζ and the vertical velocities $w(0)$ are related *as* $w(0) = \mathrm{d}\zeta/\mathrm{d}t$, which can be approximated by

$$w(0) \approx \frac{\partial \zeta}{\partial t}, \tag{3.27}^d$$

if $|u_j \partial\zeta/\partial x_j| \ll \partial\zeta/\partial \mathrm{d}t$ for $j = 1, 2$. Scaling considerations imply that this is possible only when the frequency of motion satisfies $\omega > \omega_0$, where $\omega_0 \sim u_H/L_H$ or in non-dimensional form $\omega > \omega_0^n$, where ω_0^n is a constant cutoff frequency. In the context of present work, (3.27) is expected to be satisfied for all linear waves with $\omega > \omega_c$ and part of the nonlinear waves with $\omega_0 < \omega < \omega_c$. The experiments and visualization of McGrath *et al.* (1997) show that low-frequency waves have horizontal scales of the order L_H and they are advected with the speed of the large-scale eddies in the mixed layer. Based on the measurements of Hopfinger & Toly (1976) and Hannoun & List (1988), the magnitude of ω_0 can be evaluated empirically as $\omega_0^n \approx 0.14$, with estimated values varying in the range 0.09–0.2.

The above considerations suggest that for $\omega > \omega_0$, $\psi^d(\omega) \approx \omega^2 \psi_{33}(\omega, 0)$. Further, because of the requirement that the variance of interfacial distortions

$$\overline{\zeta^2} = \int_{-\infty}^{+\infty} \psi^d(\omega) \mathrm{d}\omega \tag{3.28}$$

is finite, it is possible to expect that $\psi^d =$ constant for $\omega < \omega_0$. Thus the following spectral form can be proposed for the frequency spectrum of interfacial distortions:

$$\psi^d(\omega) = \begin{cases} \psi_{33}(\omega, 0)/\omega^2 & \text{for} \quad \omega > \omega_0 \\ \psi_{33}(\omega, 0)/{\omega_0}^2 & \text{for} \quad \omega > \omega_0. \end{cases} \tag{3.29}$$

† This result could also be derived by the scaling argument $(\overline{w^2})_i^{1/2} \sim \varepsilon^{1/3}(u_H/\omega_c)^{1/3}$, where it is assumed that the vertical velocity is determined by the turbulence and the resonant frequency $\omega_c \sim Riu_H/L_H$; hence, $(\overline{w^2})_i^{1/2} \sim u_H Ri^{-1/3}$.

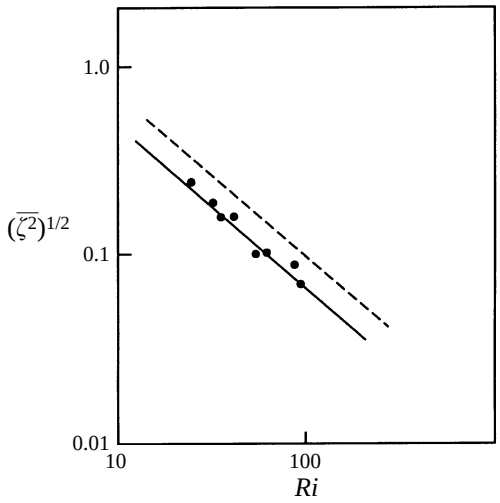

FIGURE 10. Variation of calculated and experimental non-dimensional wave amplitude with Richardson number. ——, Calculation for one-sided stirring case with $\mu_c = 0.5$; •, experimental results of Hannoun & List (1988); - - - -, calculation for the double-sided stirring case.

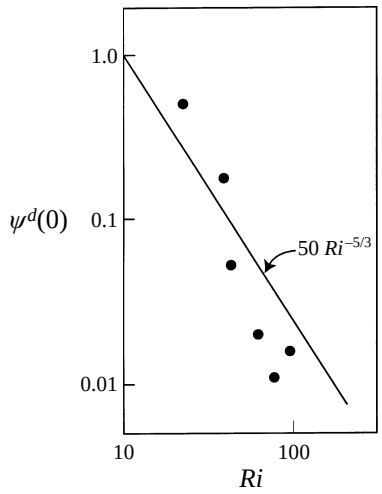

FIGURE 11. Comparison of calculated (——) and experimental (•) values of the variation of non-dimensional $\psi^d(0)$ with *Ri*.

Using (3.21), (3.24), and (3.29), it can be shown that $\psi^d(\omega) \approx g_4 Ri^{-1/3}$ for $\omega < \omega_0$, where $g_4 \approx 50$.†

The variance $\overline{\zeta^2}$, evaluated numerically using (3.28) and (3.29), is plotted in figure 10, together with the experimental data of Hannoun & List (1988) for the single-sided stirring case. A good agreement can be seen. As expected, the amplitude of oscillation for the double-sided stirring case (dashed line) is noticeably higher. Figure 11 shows a

† This is consistent with the notion that the low-frequency waves are significantly affected by the large-scale eddies near the interface and their behaviour can be specified by $\Delta b, L_H, u_H$ and ε; on dimensional grounds, the interfacial distortion spectrum for $\omega < \omega_0$ can be written as $\psi^d(\omega) \sim L_H^2 u_H^{1/3} \varepsilon^{2/3} \Delta b^{-5/3}$, or $\psi^d(\omega) \sim Ri^{-5/3}$ in non-dimensional form.

comparison of the prediction $\psi^d \approx 50Ri^{-5/3}$, for $\omega < \omega_0$, with the experimental data of Hannoun & List (1988); a fair agreement can be seen.

3.6. *Problems with the calculation of energy flux*†

The dominant processes at the interface in an overall sense are in a quasi-stationary state (or evolving slowly), because there is a balance between the energy absorbed into growing waves and their dissipation due to breaking. As such, a statistically steady-state analysis is appropriate for calculating quasi-steady-state quantities such as the r.m.s. velocities and wave amplitudes, provided that nonlinear effects which limit the wave growth and establish an equilibrium state are accounted for (as was done in §§ 3.4 and 3.5). However, a different approach using an unsteady analysis is necessary to study the energy flux into the interface, because the forcing by the turbulence leads to the growth of the waves until their amplitudes are limited by the action of dissipative mechanisms. In the nonlinear model, this dissipative mechanism was implicitly assumed to be wave breaking but it does not reveal how the energy is absorbed and dissipated. It simply gives an estimate of the amount of energy that can be sustained in the quasi-stationary state, as the following analysis demonstrates.

The energy flux across a given horizontal plane in the stratified layer is given by $\overline{pw} + \overline{w(u^2 + v^2 + w^2)}$. For linear waves, only the pressure flux $\mathscr{P} = \overline{pw}$ is significant. Therefore, the energy accumulation within the interface, for mode 1 oscillations is $-(\overline{p_+ w_+} - \overline{p_- w_-}) = -\overline{(p_+ - p_-)w(0)} = -\overline{\Delta p w(0)}$. Integration of (3.4) across the interface and combining the result with (3.2) gives

$$\frac{\Delta p}{\rho_0} = \int_{-\infty}^{+\infty} \Delta\hat{p} \mathrm{e}^{\mathrm{i}(k_1 x + k_2 y - \omega t)} \mathrm{d}k_1 \mathrm{d}k_2 \mathrm{d}\omega, \tag{3.30}^d$$

where

$$\Delta\hat{p} = \Delta b \hat{\zeta}(0) = \frac{\mathrm{i}\Delta b \hat{w}(0)}{\omega}. \tag{3.31}^d$$

Hence, $\Delta\hat{p}^{\ddagger}\hat{w}(0) = \mathrm{i}\Delta b \hat{w}^{\ddagger}(0)\hat{w}(0)/\omega$ and the joint horizontal wavenumber–frequency spectrum of $\overline{\Delta p w(0)}$ is determined in terms of the vertical velocity spectrum given by (3.17) and (3.24) as

$$\Xi_{pw}(k_1, k_2, \omega, 0) = \mathrm{i}\frac{\Delta b}{\omega} \int_{-\infty}^{+\infty} M^{\ddagger}_{3\ell} M_{3n} \chi_{ln} \, \mathrm{d}k_3 \tag{3.32a}^d$$

$$= \mathrm{i}\frac{\Delta b}{\omega} \Xi_{33}(k_1, k_2, \omega, 0). \tag{3.32b}^d$$

Further integration of (3.32) over k_1 and k_2 leads to the non-dimensional frequency spectrum of $\overline{pw}$:

$$\psi_{pw}(\omega, 0) = \mathrm{i}\frac{Ri}{\omega} \psi_{33}(\omega, 0). \tag{3.33}$$

The above expression clearly shows that in the realm of steady linear theory there cannot be any energy transfer into the interface (the integral of (3.33) over the frequency space is zero). This physically means that steady inviscid waves do not absorb energy. Thus, an unsteady analysis is required to calculate the energy flux into the interface, which will be developed in § 4.

† The authors wish to thank Dr D. J. Carruthers for pointing out this aspect, which led to the development of the unsteady model described in § 4.

4. Unsteady model

Consider the flow configuration pertinent to figure 1(*b*). The flows above and below the interface are given by (3.8) and (3.9), and the undistorted turbulence is specified by the four-dimensional Fourier transform (2.4). Now it is possible to seek unsteady solutions for the distorted flow fields using Fourier transforms of the form

$$u_j(\boldsymbol{x},t)=\int_{-\infty}^{+\infty}\int_{-\infty}^{+\infty}\hat{u}_j(k_1,k_2,z,t)\mathrm{e}^{\mathrm{i}(k_1x+k_2y)}\mathrm{d}k_1\mathrm{d}k_2, \tag{4.1}^d$$

$$\varphi(\boldsymbol{x},t)=\int_{-\infty}^{+\infty}\int_{-\infty}^{+\infty}\hat{\varphi}(k_1,k_2,z,t)\mathrm{e}^{\mathrm{i}(k_1x+k_2y)}\mathrm{d}k_1\mathrm{d}k_2, \tag{4.2}^d$$

where $j=1,2,3$, with $\hat{u}_3=\hat{w}$. Now the matching conditions at the interface are required, analogous to (3.6) and (3.7). Note that although the kinematic condition (3.6*b*) remains the same, the dynamical condition needs to be revised in view of the unsteadiness. Thus, (3.3) can be integrated across the interface to yield

$$\frac{\partial^2}{\partial t^2}\left[\left(\frac{\partial\hat{w}}{\partial z}\right)_{(z=h/2)}-\left(\frac{\partial\hat{w}}{\partial z}\right)_{(z=-h/2)}\right]=\Delta bk_{12}^2\hat{w}(k_1,k_2,0,t). \tag{4.3a}^d$$

This, together with

$$\hat{w}(k_1,k_2,h/2,t)=\hat{w}(k_1,k_2,-h/2,t) \tag{4.3b}^d$$

can be used to obtain the relationships between $\hat{u}_i, S_i^H$ and $\hat{\varphi}$. The use of $\nabla^2\varphi=0$ leads to $\hat{\varphi}\sim\mathrm{e}^{\pm k_{12}z}$ for $z<0$, based on which a transfer function between $\hat{\varphi}$ and S_3^H can be conveniently defined as

$$\left\{\begin{array}{c}\hat{\varphi}_u(k_1,k_2,z,t)\\ \hat{\varphi}_l(k_1,k_2,z,t)\end{array}\right\}=\int_{-\infty}^{+\infty}\int_{-\infty}^{+\infty}\left\{\begin{array}{c}A(\boldsymbol{k},\omega,t)\mathrm{e}^{-k_{12}z}\\ B(\boldsymbol{k},\omega,t)\mathrm{e}^{k_{12}z}\end{array}\right\}S_3^H(\boldsymbol{k},\omega)\mathrm{d}k_3\mathrm{d}\omega, \tag{4.4}^d$$

where the subscripts u and l represent upper and lower layers, respectively. This can be combined with the relationships between $\hat{u}_i, S_i^H$ and $\hat{\varphi}$ which, after the elimination of $A(k,\omega,t)$, gives an equation of the form

$$\frac{\partial^2 B}{\partial t^2}+\omega_1^2B=\lambda\mathrm{e}^{-\mathrm{i}\omega t}, \tag{4.5}^d$$

where $\omega_1^2=\Delta bk_{12}/2$ and $\lambda=\omega^2(1+\mathrm{i}k_3/k_{12})/2k_{12}$ for the single-sided stirring case. As was done in § 3.2.2, a similar expression is possible for the double-sided case, but now the upper- and lower-layer contributions should be considered separately and the condition $\overline{S_{3(+)}^H S_{3(-)}^H}=0$ should be used. For example, analogous to (4.4), now $\hat{\varphi}_u$ takes the form

$$\hat{\varphi}_u(k_1,k_2,z,t)=\int_{-\infty}^{+\infty}\int_{-\infty}^{+\infty}\left(M_1(\boldsymbol{k},\omega,t)S_{3(+)}^H(\boldsymbol{k},\omega)+M_2(\boldsymbol{k},\omega,t)S_{3(-)}^H(\boldsymbol{k},\omega)\right)\mathrm{e}^{-kz}\mathrm{d}k_3\mathrm{d}\omega, \tag{4.6}^d$$

where M_1 and M_2 are functions.

The solution to (4.5) becomes

$$B\sim\mathrm{e}^{\pm\mathrm{i}\omega_1 t}+\lambda\mathrm{e}^{-\mathrm{i}\omega t}/(\omega_1^2-\omega^2)\quad\text{for}\quad\omega_1\neq\omega \tag{4.7a}^d$$

and for the resonant condition

$$B\sim\mathrm{e}_1{}^{\pm\mathrm{i}\omega_1 t}+\mathrm{i}\lambda t\mathrm{e}^{-\mathrm{i}\omega t}/2\omega_1\quad\text{for}\quad\omega_1=\omega. \tag{4.7b}^d$$

The constants of integration can be evaluated using the initial conditions $\partial\hat{\varphi}/\partial z = 0$ and $(\partial/\partial t)(\partial\hat{\varphi}/\partial z) = 0$ at $t = 0$. Thus the linear unsteady theory predicts algebraic growth of frequencies that satisfy $\omega = \omega_1 = (\Delta b k_{12}/2)^{1/2}$. Recall that these are the same resonant modes identified in the steady analysis presented in § 3.2.1.

It is possible to estimate the energy input to the growing linear waves using an approach similar to that discussed in § 3.6. Integration of (3.4) in time across the interface gives

$$\frac{\Delta p}{\rho_0} = -\Delta b \int_0^t w(0)\mathrm{d}t. \tag{4.8}^d$$

Using the Fourier representation

$$\frac{\Delta p}{\rho_0} = \int_{-\infty}^{+\infty}\int_{-\infty}^{+\infty} \Delta\hat{p}(k_1, k_2, z, t)\mathrm{e}^{\mathrm{i}(k_1 x + k_2 y)}\mathrm{d}k_1\mathrm{d}k_2, \tag{4.9}^d$$

and introducing the transfer functions θ and $\mathscr{V}$

$$\hat{w}(k_1, k_2, 0, t) = \int_{-\infty}^{+\infty}\int_{-\infty}^{+\infty} \theta(\boldsymbol{k}, \omega, t) S_3^H(\boldsymbol{k}, \omega)\mathrm{d}k_3\mathrm{d}\omega, \tag{4.10a}^d$$

and

$$\int_0^t \hat{w}(k_1, k_2, 0, t) = \int_{-\infty}^{+\infty}\int_{-\infty}^{+\infty} \mathscr{V}(\boldsymbol{k}, \omega, t) S_3^H(\boldsymbol{k}, \omega)\mathrm{d}k_3\mathrm{d}\omega, \tag{4.10b}^d$$

it is possible to evaluate the joint horizontal wavenumber spectra as

$$\Xi_{pw}(k_1, k_2, 0, t) = -\Delta b \int_{-\infty}^{+\infty}\int_{-\infty}^{+\infty} \mathscr{V}(\boldsymbol{k}, \omega, t)\theta(\boldsymbol{k}, \omega, t)\chi_{33}(\boldsymbol{k}, \omega)\mathrm{d}k_3\mathrm{d}\omega. \tag{4.11}$$

In calculating θ and $\mathscr{V}$, both inviscid oscillatory (4.7*a*) and growing (4.7*b*) solutions should be considered, although on physical grounds one might expect that oscillatory solutions may not absorb energy. This can be readily demonstrated by considering the worst-case scenarios, the large-amplitude oscillatory solutions that are expected in the neighbourhood of $\omega = \omega_1$. Using (3.8), (4.4), (4.7*a*) and (4.11), it is possible to evaluate $\Xi_{pw}(k_1, k_2, 0, t)$, which, in turn, can be integrated over k_3 and ω to obtain the contribution to $\overline{\Delta p w(0)}/\rho_0$ of waves with $\omega \neq \omega_1$ but $\omega \approx \omega_1$. The resulting solution can be expressed as

$$\overline{\Delta p w(0)} \sim \mathrm{Re}\left(i\frac{Ri}{4}\omega_1 \int_{-\infty}^{+\infty}\int_{-\infty}^{+\infty}\int_{-\infty}^{+\infty}\int_{-\infty}^{+\infty} k^2 \frac{\sin^2(\omega' t/2)}{\omega'}\chi_{33}(\boldsymbol{k}, \omega)\mathrm{d}\boldsymbol{k}\,\mathrm{d}\omega\right) = 0, \tag{4.12}$$

for single-sided stirring, where we have used $\omega = \omega_1 + \omega'$, with small ω', and have utilized the standard limit of the Fourier integral, as $t \to \infty$, $\int_{-\infty}^{+\infty} F(\omega')(\sin\omega' t/\omega')\mathrm{d}\omega' \to \pi F(0)$. The corresponding expression for the double-sided stirring also shows similar behaviour.

Nonetheless, resonant interfacial waves of frequency $\omega_1 = (\Delta b k_{12}/2)^{1/2}$ absorb energy from the adjacent turbulent layer. Combining the solution (4.7*b*) for $\omega = \omega_1$ with (4.4), (3.8) and (4.11), it is possible to calculate the pressure–velocity correlation spectra. Since this solution contains both temporally oscillatory and growing terms, suitable averaging should be performed when estimating the rate of mean energy absorption into the interface. Since the waves are expected to become strongly nonlinear and transfer energy between different frequencies (or sometimes break) within one oscillatory period, a suitable choice would be to average over a single

wave oscillation, namely

$$\langle f \rangle = \frac{1}{2\pi/\omega} \int_0^{2\pi/\omega} f(\omega, t) \mathrm{d}t, \tag{4.13}$$

where f is a statistical function that has an oscillatory behaviour with frequency ω. The averaged pressure–velocity correlation spectra can thus be evaluated as

$$\langle \Xi_{pw}(k_1, k_2, 0) \rangle = \frac{\pi}{4} \Delta b \int_{-\infty}^{+\infty} \int_{-\infty}^{+\infty} k_{12}^2 \, |\lambda|^2 \, \chi_{33}^H(\boldsymbol{k}, \omega) \mathrm{d}k_3 \mathrm{d}\omega. \tag{4.14}$$

It should be noted that the frequencies in (4.14) are the resonant frequencies specified by $\omega_1 = (\Delta b k_{12}/2)^{1/2}$, and hence the integration should be performed over these selected frequencies. This complicated integral can be somewhat simplified by specifying χ_{33}^H in terms of the three-dimensional spectrum ϕ_{33} modified by the Dirac delta function $\delta[\omega - (\Delta b k_{12}/2)^{1/2}]$ to allow the treatment of specific frequencies, instead of using (2.1). The spectra $\langle \Xi(k_1, k_2, 0) \rangle$ so obtained can be integrated over k_1 and k_2 to yield the energy absorbed into the linear wave field ($\omega > \omega_c$) as

$$\mathscr{P} = -\overline{\Delta p w(0)} \approx g_5 R i^{-n}, \tag{4.15a}$$

where $g_5 = (3\sqrt{2}\pi^2 g_3 A/28), A = 2.4$ (a constant evaluated by numerical integration) and $n = 2/3$. The energy absorbed into the wave field at $\omega > \omega_c$ is assumed to distribute rapidly to maintain the spectral form (3.24). A similar analysis carried out for the double-sided stirring case gives

$$\mathscr{P} = g_6 R i^{-n}, \tag{4.15b}$$

where $g_6 = 2g_5$ (i.e. twice that for the single-sided case) and $n = 2/3$.

5. The entrainment model

Here we apply the results of energy flux calculations (4.15) to estimate the rate of entrainment at a shear-free density interface for single- and double-sided stirring cases shown in figures 12(*a*) and 12(*b*), respectively. For calculational simplicity the origin of the coordinate system for the single-sided case has been shifted. The depth of the turbulent layer(s) is taken as D. The mean densities (buoyancies) ρ_1 and ρ_2 (b_1 and b_2) of upper and lower layers are taken as uniform. Based on the previous laboratory experiments of Crapper & Linden (1974), Fernando & Long (1985) and E & Hopfinger (1986), the interface is assumed to have a linear density (buoyancy) profile with a buoyancy jump of Δb and the thickness of the interface h is taken as $h = \alpha D$, where α is a constant. In practical situations, the interfacial thickness is determined by the mixing that occurs within the interface; why it should be a constant fraction of the mixed-layer depth (or the integral length scale) is not addressed in the present work. Further studies are required to understand such details.

If turbulence is applied, for example at $t = 0$, the potential and kinetic energies within the interface are expected to grow. While the interfacial motions are small, this growth can be described by

$$\frac{\partial}{\partial t}\left(u_i^2 + \frac{b^2}{2N^2}\right) + \frac{\partial (p u_i)}{\partial x_i} = 0, \tag{5.1}^d$$

where b is the fluctuation of buoyancy. However, wave breaking limits the amplitude of waves thus establishing a quasi-steady state. As mentioned, laboratory experiments

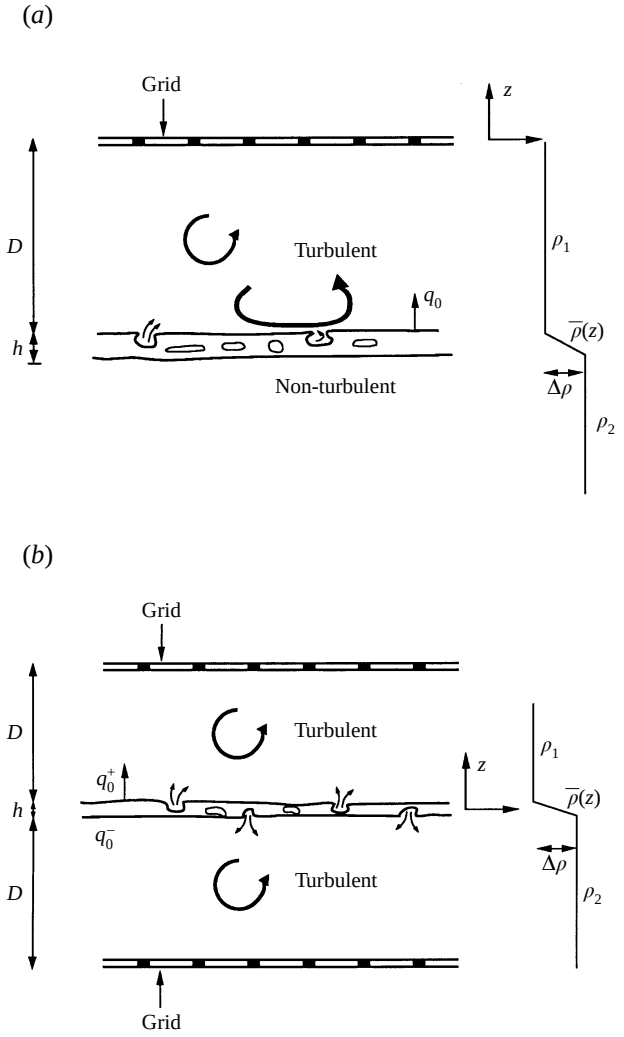

FIGURE 12. Schematic diagrams of (*a*) single- (*b*) double-sided stirring experiments with oscillating-grid turbulence.

show that these breaking events are temporally and spatially intermittent and lead to the formation of turbulent patches at the interface via which small-scale mixing takes place. Then the mixed fluid in these patches is scoured by the eddies of the turbulent layer, and eventually homogenized into the turbulent layer.

Let us assume that the intermittency factor of the 'patches' is $I_n (0 < I_n < 1)$, and the dissipation rate ε_p and the buoyancy flux $q_p (= -\overline{bw})$ within each patch determine the horizontally averaged rate of dissipation $\varepsilon(z)$ and buoyancy flux $q(z)$ within the interface. Long (1978), using a detailed scaling analysis, showed that $q = I_n q_p$ and $\varepsilon = I_n \varepsilon_p$, and $q_p \propto \varepsilon_p$ or $q \propto \varepsilon$. Within the patches, small-scale turbulence and molecular processes lead to the dissipation of kinetic energy and conversion of kinetic energy into the buoyancy flux $\overline{bw}$. Some patches occur at the entrainment interface, thus contributing directly to the mixing of fluid below the interfacial layer with that above it, i.e. generating a buoyancy flux into the turbulent layers, whereas

smaller patches occurring within, and their gravitational collapse, are responsible for maintaining a smooth buoyancy profile within the interface (while maintaining a small but finite thickness). Once an overall quasi-steady state is reached, the horizontal (ensemble)-averaged energy equation for the interfacial region can be written as

$$\frac{\partial}{\partial z}\left(\overline{pw} + \overline{w(u^2+v^2+w^2)}\right) + q(z) + \varepsilon(z) = 0. \tag{5.2}$$

If $q \propto \varepsilon$, then the mixing efficiency $\eta = q/(q+\varepsilon)$ within the patches and in the interfacial layer should be a constant, although, in general, η is dependent on the bulk Richardson number of stratified turbulence (Linden 1979, 1980). The constant mixing efficiency (≈ 0.2) of continuously forced, stratified turbulent flows has also been demonstrated in the experiments of McEwan (1983) (also see Hunt, Stretch & Britter 1986). In addition, since the turbulent patches in the interface grow such that vertical inertia and buoyancy forces are of the same order, the averaged local Richardson number in the patches should be of order one, and hence according to mixing efficiency curves (e.g. Fernando 1991), $\eta \approx 0.2$ is expected. This result of constant η, together with the integration of (5.2) across the interface and the assumption that the energy flux into the interface is dominated by $\overline{pw}$ gives

$$\mathscr{P} = -\overline{\Delta p w(0)} \approx \frac{1}{\eta}\int_{-(D+h)}^{-D} q(z)\mathrm{d}z. \tag{5.3}$$

The latter assumption is corroborated by the measurements of Hannoun *et al.* (1988). They found that the gradient of the vertical TKE flux at or near the interface is very small (see their figure 9). Further discussion on this aspect is given by Wijesekera, Dillon & Padman (1993).

5.1. *Single-sided stirring case*

The entrainment rate for the single-sided stirring case is usually defined as the *rate of movement of the interface*,

$$E_b = -\frac{\partial D}{\partial t}. \tag{5.4}^d$$

If there is a fixed mass in the whole volume, entrainment leads to the increase in the density of the turbulent region (figure 12*a*). It can be shown (see § 5.1) that, in this case, the entrainment velocity E_b can also be written as

$$E_b = \frac{D}{\Delta b}\frac{\partial \overline{b_1}}{\partial t} = \frac{D}{\Delta b}\frac{\partial \Delta b}{\partial t}. \tag{5.5}^d$$

The buoyancy profile for the single-sided case is shown in figure 12(*a*), and can be written as

$$\bar{b}(z) = \begin{cases} b_1, & z > -D \\ b_1 + \dfrac{\Delta b}{h}(z+D), & -D > z > -(D+h) \\ b_2, & -(D+h) > z. \end{cases} \tag{5.6}^d$$

The equation for the conservation of buoyancy

$$\frac{\partial b}{\partial t} = \frac{\partial q}{\partial z}, \tag{5.7}^d$$

can be integrated in conjunction with (5.6), in the regions $-(D+h)$ to 0, $-D$ to 0 and $-(D+h)$ to z, to yield

$$\Delta b\left(\tfrac{1}{2}h + D\right) = \Delta b D(1+\alpha/2) = \text{constant}, \tag{5.8}^d$$

$$q_0 = -D\frac{\partial \Delta b}{\partial t} = -E_b \Delta b, \tag{5.9}^d$$

and

$$q(z) = q_0 + (z+D)\frac{\partial \Delta b}{\partial t} + \frac{1}{2\alpha}(z^2 - D^2)\frac{\partial (\Delta b/D)}{\partial t} + \frac{z+D}{\alpha}\frac{\partial \Delta b}{\partial t}, \tag{5.10}^d$$

respectively, where $q_o = q(-D)$ and $q[-(D+h)] = 0$.

Using (5.3), (5.10) and (4.15*a*), and after some algebra, it is possible obtain

$$\mathscr{P} = g_5 u_H^3 Ri^{-n} = \frac{1}{\eta}\beta q_0 D = -\frac{\beta}{\eta} D \Delta b E_b, \tag{5.11}^d$$

where $\beta = \alpha(\alpha+3)/6$. When comparing (5.11) with previous oscillating-grid mixing-box experiments, it is possible to use the widely used empirical result for homogeneous turbulence, $L_H = \alpha_1 D$ (Thompson & Turner 1975; Hopfinger & Toly 1976). This, together with (5.11), gives

$$\mathscr{E}_b = \frac{|E_b|}{u_H} = \left(\frac{g_5 \eta \alpha_1}{\beta}\right) Ri^{-(1+n)} \tag{5.12}^d$$

where $\mathscr{E}$ is the boundary entrainment coefficient.

It should be noted that n and g_5 are sensitive to the model used for the undistorted homogeneous turbulence. In addition, g_5 is sensitive to the wave growth and breaking criterion employed and to the period over which the energy is fed into a particular wave. Keeping such caveats in mind, the entrainment law for the single-sided stirring case can be written in the form

$$\mathscr{E}_b = \frac{|E_b|}{u_H} = K Ri^{-n_1}, \tag{5.13}^d$$

where K is a constant. Comparison of (5.13) with experimental results is not a straightforward task because, in most of the reported experiments, detailed quantities such as α and α_1 have not been measured and hence the constants required to evaluate K are not available. Most reported studies have used available adjustable constants derived from a few other studies, which often vary from one study to another. Because the study of Hannoun & List (1988) covers a comprehensive set of measurements, here we use their constants to evaluate n_1 and K. Using $g_3 = 0.0951$ (§2), $n = 2/3$ (§4), $h/L_H \approx 0.03$ (McGrath *et al.* 1997), $\alpha_1 \approx 0.1$ (Hannoun & List 1988) and $\eta \approx 0.2$ (McEwan 1983), $g_5 \approx 0.34, n_1 = 5/3$ and $K \approx 4.5$ are obtained. This prediction (dashed line) is depicted in figure 13(*a*) together with the experimental data of Hannoun & List (1988); the agreement is good. E & Hopfinger (1986) reported an entrainment law with $n_1 \approx 1.5$ and $K \approx 3.8$, which is also not far from the values predicted here.

It should be noted that the entrainment law (5.13) is only valid in the Ri range where wave breaking is the dominant mixing mechanism. According to McGrath *et al.* (1997) and Hannoun *et al.* (1988), in shear-free turbulent mixing, the wave breaking is prominent in the range $30 < Ri < 100$, and hence (5.13) should only be compared with the data in this range. Some of the previously reported n_1 values have been obtained by considering data well outside from this range, which should be kept in mind in comparing them with the predictions. Previously reported values vary in the range $1.2 < n_1 < 1.75$, with the recent oscillating grid experiments of Huppert, Turner & Hallworth (1995) reporting $n_1 \approx 1.7$.

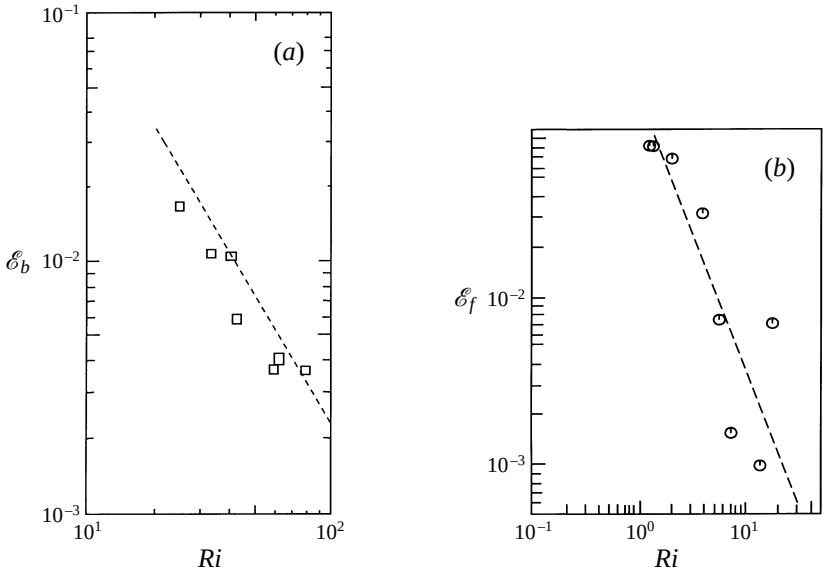

FIGURE 13. (*a*) A plot of boundary entrainment coefficient $\mathscr{E}_b$ versus the Richardson number *Ri*, adopted from Hannoun & List (1988) and the dashed line representing the entrainment law $\mathscr{E} \approx 4.5Ri^{-5/3}$ estimated from the present model for the single-sided stirring case. (*b*) A plot of the flux entrainment coefficient $\mathscr{E}_f$ versus Richardson number, obtained from Jayesh *et al.* (1991). The dashed line represents the estimate made using the present model for the double-sided stirring case.

5.2. *Double-sided stirring case*

For the double-sided stirring case, the interface does not move but there is a flux of matter across the interface. Therefore, another measure of entrainment is used, namely the *entrainment flux velocity* defined as (Turner 1968)

$$E_F = \frac{\text{buoyancy flux}}{\Delta b} = -\frac{D}{\Delta b}\frac{\partial \overline{b_2}}{\partial t} = \frac{D}{\Delta b}\frac{\partial \overline{b_1}}{\partial t}. \tag{5.14}^d$$

Since $\Delta b = (b_1 - b_2)$, E_F can also be expressed in terms of the change of the buoyancy jump as

$$E_F = \frac{D}{2\Delta b}\frac{\partial \Delta b}{\partial t}. \tag{5.15}^d$$

Note that E_b and E_F are the same if the change in layer buoyancies in the double-sided case is the same as for the case where the opposite side is not turbulent. Then Δb decreases twice as fast as in the former case and the entrainment rates become equal. In general, this need not be the case since the interfacial structure (e.g. buoyancy flux profiles) in the two cases is different.

A schematic of the two-sided stirring set-up is given in figure 12(*b*). The buoyancy profiles within the layers are also given by (5.6), but the buoyancies in both layers are now time dependent; however, it is easily shown, using buoyancy conservation for the whole fluid system, that $b_1 + b_2$ should remain constant. Integration of (5.7) across the turbulent layers and part of the interfacial layer gives the buoyancy fluxes at the upper and lower entrainment interfaces, q_o^+ and q_o^-, and within the interface $q(z)$, as

$$q_0^+ = q_0^- = -D\frac{\partial \overline{b_1}}{\partial t} = D\frac{\partial \overline{b_2}}{\partial t} \tag{5.16}^d$$

and

$$q(z) = q_0^- + \frac{1}{2h}\left(z^2 + \frac{h^2}{4}\right)\frac{\mathrm{d}\Delta b}{\mathrm{d}t}. \tag{5.17}^d$$

Using (5.3) and (5.17), $\mathscr{P}$ can be calculated as

$$\mathscr{P} = -D\alpha(1 + \alpha/6)E_F\Delta b, \tag{5.18}^d$$

which, when combined with (4.15b), gives the entrainment law

$$\mathscr{E}_f = \frac{E_F}{u_H} = K^* Ri^{-n_1}, \tag{5.19}^d$$

where $K^* = g_6\eta\alpha_1/\alpha(1 + \alpha/6)$ and $n_1 = 5/3$.

An interesting result emerges from the comparison between (5.19) and (5.13). For the single-sided stirring case, $K = g_5\eta\alpha_1/\beta = g_5\eta\alpha_1[\alpha(\alpha + 3)/6]$, whereas for the double-sided stirring case $K^* = g_6\eta\alpha_1/[\alpha(1 + \alpha/6)]$. Since $\alpha(= h/D)$ is small and $g_6 \approx 2g_5, K \approx K^*$. This result is confirmed by the laboratory experiments of Turner (1968), who found that the entrainment rate of the double-sided stirring case is approximately the same as that of the single-sided stirring case, with the difference between the two being within the error margin of the experiments.

An interesting set of data on double-sided entrainment across shear-free density interfaces can be retrieved from Jayesh, Yoon & Warhaft (1991) (see also Jayesh & Warhaft 1994). They investigated the evolution of turbulence in a two-layer heat-stratified uniform mean flow past a grid in a standard wind tunnel set-up. The turbulence induced on either side of the interface caused mixing across the interface. The flow in each downstream location was stationary. This situation is equivalent to the double-sided stirring considered here, and E_F can be evaluated using (5.14). The flow visualization studies (their figure 7) show that the interface is dominated by the first mode of internal waves, but the interfacial thickness is much larger with typically $\alpha \approx 0.1$, thus yielding $g_6 \approx 0.7$ and $K^* \approx 0.14$. A plot of E versus Ri is shown in figure 13(b), with the dashed line corresponding to $K^* \approx 0.14$ and $n_1 = 5/3$. A good agreement can be seen. A set of experiments similar to that of Jayesh *et al.* (1991) has been conducted in a two-layer salt-stratified water channel by Huq & Britter (1995). Their experiments cover the range $0.1 < Ri < 18$ and clearly show transition to $Ri^{-5/3}$ behaviour at $Ri > 10$.

Finally, the differences between single- and double-sided stirring are worth noting. First, the energy flux that can be absorbed into the interface is different for the two cases, because of the differences in the velocity fields. Second, the amount of TKE expended to transport buoyancy flux through the interface is different because of the differences in the buoyancy flux profiles through the interfacial layer, as evident from (5.10) and (5.17).

6. Turbulence in the mixed layer

Turbulence statistics above (and below) the interface for finite Ri can be derived by extending the model discussed above (with a further assumption) to relate the wavenumber and frequency spectra in the nonlinear range ($\omega < \omega_c$). A simplified analysis can be presented, however, without such assumptions if the case $Ri \to \infty$ (so that the interface is rigid) is considered. Then the analysis of Hunt (1984) for shear-free boundary layers can be adopted and extended.

When the boundary condition $w = 0$ is imposed on $z = 0$, it can be shown that

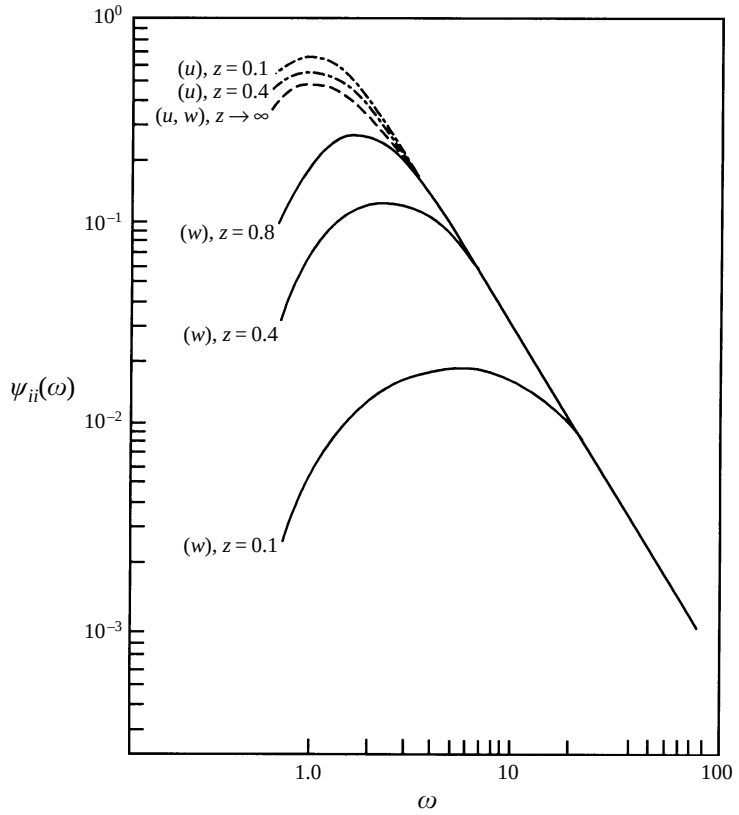

FIGURE 14. Horizontal ($u_1 = u$) and vertical ($u_3 = w$) normalized energy spectra in the frequency domain, calculated for various normalized distances (z) from the surface (in the limit $Ri \to \infty$).

(3.10) is still applicable with

$$\boldsymbol{M} = \begin{pmatrix} e^{ik_3 z} & 0 & \dfrac{ik_1}{k_{12}} e^{-k_{12} z} \\ 0 & e^{ik_3 z} & \dfrac{ik_2}{k_{12}} e^{-k_{12} z} \\ 0 & 0 & e^{ik_3 z} - e^{-k_{12} z} \end{pmatrix}. \tag{6.1}$$

Using (3.17) and (2.1)–(2.7), (6.1) can be used to evaluate the frequency spectra for u and w, $\psi_{11}(\omega, z)$ and $\psi_{33}(\omega, z)$, as functions of z. The results are plotted in figure 14. Note that the spectra are not accurate at low $\omega (\omega < 1)$, as mentioned in § 2. Nonetheless, the modification of velocity statistics due to the presence of the rigid surface (i.e. reduction of w and increase of u) is very clear.

Note that, in the present analysis, the amplification of u and the reduction of w at low frequencies is a kinematic effect. The induced irrotational field mainly contains large-scale motions, so that the additive effect is mainly felt at large scales (small frequencies) while the small scales remain undistorted. The vortex structures of the homogeneous turbulence thus remain unchanged by the introduction of the interface, and the flow around these structures is modified by irrotational fluctuations. On the other hand, Long (1978) argued that the eddies of integral scales can flatten at the

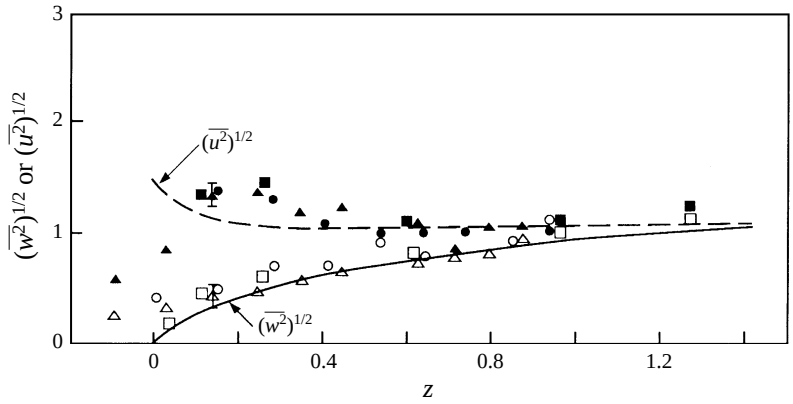

FIGURE 15. Comparison of the mixed-layer turbulence data of Hannoun *et al.* (1988) and the calculations based on the present model. Filled symbols and broken line, horizontal component, open symbols and dark line, vertical component. △, $Ri = 100$; ○, $Ri = 70$ and □, data taken near a flat plate. All data have been normalized.

interface thus squashing them vertically and transferring energy from the vertical to horizontal components; here, the flattening of eddies involves changes of vortex structures near the interface. An analysis based on Long's notion requires estimations of the changes induced by vortex stretching and compression. Some estimates of velocity changes that occur due to the distortion of vortex motions are given in Hunt (1984).

The normalized vertical and horizontal r.m.s. velocities were calculated using $\psi_{33}(\omega, z)$ and $\psi_{11}(\omega, z)$; the results are shown in figure 15, together with the measurements of Hannoun *et al.* (1988) at finite Ri and $Ri \to \infty$. A good agreement can be seen between the calculations and measurements at large z; discrepancies observed close to the surface can be attributed to the use of potential flow theory, which neglects the viscous drag on the horizontal motions and the distortion of vortex structures near the interface, and to the presence of interfacial oscillations at finite Ri.† A detailed discussion on these aspects is given in Kit *et al.* (1997).

It is also possible to evaluate the spectrum of velocity shear $\partial u_i/\partial z$ using expressions analogous to (3.10) and (3.17); the result is

$$\Xi_{ij}^{S}(k_1, k_2, z, \omega) = \int_{-\infty}^{+\infty} N_{il} N_{jn} \chi_{ln}^{H} \mathrm{d}k_3, \tag{6.2}$$

where $N_{ij} = \partial M_{ij}/\partial z$. For the case of $z = 0$, we find the corresponding frequency spectra as

$$\psi_{11}^{S}(\omega, 0) = \psi_{22}^{S}(\omega, 0) = \frac{8\pi g_3 \omega^6}{3\left(g_2 + \omega^2\right)^{17/6}}. \tag{6.3}$$

† A detailed calculation shows that the effect of interfacial motions on turbulence statistics can be neglected at distances $z/L_H \gg Ri^{-1}$, and in this limit the $Ri \to \infty$ solution is valid. For example, the one-dimensional wavenumber spectrum $\Theta_{33}(k_1, z)$ can be derived as $\Theta_{33}(k_1, z) = \Theta_{r\to\infty 33}(k_1, z) + a_1 \mathrm{e}^{-a_2 (z/L_H) Ri}$, where a_1 and a_2 are constants.

Note that the shear induced by high-frequency motions is pronounced. In a model based on scaling arguments, Mory (1991) assumed that K–H instabilities that develop owing to the sloshing of turbulent eddies over the interface are responsible for local mixing at the interface. Since the present analysis is based on overall statistics, it is not possible to check the individual contributions of the 'eddies' in an explicit way. Nevertheless, as Tennekes & Lumley (1973, p. 258) have argued, it is possible to assume that a combination of Fourier 'waves', with wavenumbers lying between $0.62k$ and $1.62k$, is a good representation for conceptual isolated 'eddies of wave number k'. The magnitude of shear exerted by eddies of wavenumber k can thus be estimated as

$$S_k^2 = \left[\left(\frac{\partial u_1}{\partial z}\right)^2 + \left(\frac{\partial u_2}{\partial z}\right)^2\right]_k \approx \int_{0.62\omega}^{1.62\omega} \psi_{\alpha\alpha}(\omega, 0)\mathrm{d}\omega; \quad \alpha = 1, 2, \tag{6.4}$$

and the maximum shear appears to be exerted by the eddies with frequencies near the Kolmogorov frequency $\omega_c = (\varepsilon/\nu)^{1/2}$. The pertinent local gradient Richardson number becomes

$$Ri_g = \frac{N^2}{S_k^2} \approx \frac{\gamma Ri Re^{-2/3}}{3.28\ C_1^{2/3}}, \tag{6.5}$$

where $\gamma = L_H/h, Re = u_H L_H/\nu$ is the Reynolds number and C_1 was defined in § 2. If it is assumed that K–H instabilities originate when Ri_g drops below a critical value Ri_{gc}, (6.5) can be used to determine the possibility of such instabilities at the interface. In the linear stability analysis of unbounded stratified shear flows, $Ri_{gc} = 1/4$; the critical value for bounded flows can be less (Fernando 1991). Assuming that the linear-theory-based values are still applicable to the perturbations of the interface (e.g. Phillips 1977, p. 218), it is possible to estimate the Richardson number range in which K–H instabilities are active as $Ri < 12.5$, for typical oscillating-grid experiments with $\gamma \approx 1, C_1 \approx 0.61$ and $Re \approx 100$. This result is at variance with Mory's conjecture that interfacial mixing is caused by K–H instabilities at moderate and high Ri.

Alternatively, it is possible to estimate the *total* contribution of all eddies of wavenumbers between the energy-containing scale and the Kolmogorov scale to interfacial shear as

$$\overline{\left(\frac{\partial u_1}{\partial z}\right)^2 + \left(\frac{\partial u_2}{\partial z}\right)^2} = \int_1^{\omega_c} \psi_{\alpha\alpha}^S(\omega, 0)\mathrm{d}\omega \approx 4\pi g_3 \omega_c^{4/3} \tag{6.6}$$

or

$$Ri_g \approx 0.42\ C_1^{-2/3} \gamma Ri Re^{-2/3}, \tag{6.7}$$

where Ri_g is now based on the total shear. Assuming $Ri_{gc} = 1/4$, it is possible to estimate the criterion for the formation of K–H instabilities, with the typical parameters of $Re \approx 100, \gamma \approx 1$ and $C_1 \approx 0.61$, as $R_i < 10$.

Both of the above analyses show that K–H instabilities can contribute little toward turbulent mixing at shear-free density interfaces when $Ri > 10$ or so. This inference is based on statistical analysis and does not imply that K–H events are absent altogether (see figure 5*c*). At low Ri, Linden (1973) argued that the predominant mixing mechanism is the 'splashing' of interfacial-layer fluid into the mixed layer due to impingement of eddies on the interface. If the K–H instabilities occur, they grow rather slowly (Thorpe 1985) and can often be overshadowed by other faster mechanisms; typical time scales of 'splashing' and K–H mechanisms are $Nt \sim O(1)$ (Linden 1973) and $Nt \sim O(10)$, respectively (Thorpe 1985; Lewellen & Sykes 1982).

Note that for Linden's 'splashing' mechanism to operate, the eddies of integral scale should be directly involved in entrainment by impinging on the interface and by splashing or scouring the heavy fluid out of it. At high Ri, however, the eddies are too feeble to do so, whence local interfacial instability mechanisms (for example, wave breaking) take over the entrainment process. Utilizing the oceanic Richardson number statistics of Desaubies & Smith (1982), Thompson (1984) has inferred that the direct involvement of integral-scale eddies is completely cut off when Ri_g (based on (6.6)) is greater than 1.33. For typical values of Re and γ quoted above, this means that when $Ri > 35$, the sole mixing mechanism should be the breaking of waves. This calculation matches the experimental observations of Fernando & Long (1985), Fernando (1989) and McGrath *et al.* (1997) who reported a change of entrainment characteristics at around $Ri \approx 30$–40.

7. Summary and discussion

We have developed a heuristic model based on analysis, physical arguments and limited use of experimental data for the statistics of turbulence, the generation of internal waves and their effects on turbulent mixing across sharp density interfaces subjected to shear-free turbulence. The analytical components were essentially based on the rapid distortion theory framework of Hunt (1984) and the observation that the dissipation rate of turbulent kinetic energy (ε) above a shear-free interface is independent of the height z.

Two configurations, namely, (i) a turbulent fluid layer separated from a non-turbulent heavy fluid layer by a density interface (single-sided stirring) and (ii) a density interface sandwiched between identical turbulent layers (double-sided stirring), were considered. In both cases the interface was assumed to be thin and to consist of the first mode of internal waves. Case (i) is applicable to situations of mixed-layer deepening in stably stratified water bodies due to turbulence induced by convective stirring or surface-wave breaking. The latter case is important in analysing the interfacial migrations in density step structures – for example, when a series of turbulent layers are separated by density interfaces, as in thermohaline staircases in oceans (Kelley 1987).

Both steady and unsteady analyses were performed for interfacial wave motions and surrounding turbulence. The steady analysis yielded the frequency spectrum for high-frequency waves, $\omega > \Delta b/2u_H$, and waves with $\omega < \Delta b/2u_H$ have resonant characteristics. By assuming that all waves in the resonant regime and a range of waves in the non-resonant regime satisfying $\omega < \Delta b/2\mu u_H$, where $\mu(= 1/2)$ is a constant, are subjected to breaking during their growth, a nonlinear model was constructed for the interfacial displacement spectrum. The model was used to calculate the r.m.s. velocity and interfacial distortions. The principal quantitative results are (in dimensional form)

$$\overline{w^2}/u_H^2 \approx 1.8Ri^{-1/3}, \quad \overline{\zeta^2}/L_H^2 \approx 3.2Ri^{-5/6}$$

for single-sided stirring and

$$\overline{w^2}/u_H^2 \approx 2.6Ri^{-1/3}, \quad \overline{\zeta^2}/L_H^2 \approx 4.6Ri^{-5/6}$$

for double-sided stirring.

The energy absorbed into the interface was calculated using an unsteady linear theory. This formulation also shows the presence of growing resonant modes, and the energy is absorbed into the interface via these growing waves. The other modes neither grow nor absorb energy. By using the average energy flux absorbed over one

cycle (based on linear theory), the energy flux available for entrainment was estimated, based on which a phenomenological entrainment model was developed to predict the entrainment rate across shear-free density interfaces. The results are

$$-\frac{1}{\rho_0}\overline{\Delta pw(0)} \approx 0.34u_H^3 Ri^{-2/3}, \quad E_b \approx 4.5Ri^{-5/3}$$

for single-sided stirring, and

$$-\frac{1}{\rho_0}\overline{\Delta pw(0)} \approx 0.68u_H^3 Ri^{-2/3}, \quad E_F \approx 4.5Ri^{-5/3}$$

for double-sided stirring, where the coefficients were estimated for the case of laboratory oscillating-grid experiments of Hannoun & List (1988). These entrainment-rate predictions were consistent with the experimental measurements.

The nature of turbulence in the layer adjacent to the interface was analysed in the large-Richardson number limit to predict the spectra and r.m.s. velocities. The distortion of turbulence in a layer of thickness approximately L_H was clearly evident. It was also found that this analysis is a good approximation for distances $z/L_H \gg Ri^{-1}$. Calculation of the velocity shear exerted by eddies sloshing horizontally over the interface indicated that Kelvin–Helmholtz type instabilities can be active only at low Richardson numbers ($Ri < 10$).

The analysis presented here has led to new physical concepts about the generation of waves on the interface by turbulence and their effects on mixing. It is assumed that different types of dynamical regimes at different wavenumber/frequency ranges are related to one another. This analysis has yielded quantitative results over a significant parameter range. It is likely that the model analysis presented here can be extended to other types of stratified flows where breaking waves on interfaces are generated by external turbulence and where one observes phenomena similar to those examined here. However, there are clearly some important mechanisms of mixing proposed here that should be studied in detail using nonlinear theories and numerical simulations.

The authors wish to thank Drs David J. Carruthers and Gilbert R. Stegen for their continued interest and encouragement; Drs Imad Hannoun, Marc Fleury, Jose Redondo and I. P. DeSilva for providing access to their original data; and Drs P. F. Linden, D. F. Jankowski and G. Oth for their support in numerous ways. Three anonymous referees provided valuable comments that led to significant improvements of this paper. Financial assistance for this work was provided by the Science Applications International Corporation, the National Science Foundation and the Office of Naval Research (Small-Scale Processes and High-Latitude Dynamics Programs). Part of the work was carried out when the first author was a visitor at the UK Meteorological Office, the hospitality and financial support of which are gratefully acknowledged.

REFERENCES

Bouvard, M. & Dumas, H. 1967 Application de la méthode du fil Chaud á la mesure de la turbulence dans l'eau. *Houille Blanche* **22**, 257–278.

Brekhovskikh, L. M., Konjaev, K. V., Sabinin, K. D. & Serikov, A. N. 1975 Short period internal waves in the sea. *J. Geophys. Res.* **80**, 856–864.

Carruthers, D. J. & Hunt, J. C. R. 1986 Velocity fluctuations near an interface between a turbulent region and a stably stratified layer. *J. Fluid Mech.* **165**, 475–501.

Carruthers, D. J. & Hunt, J. C. R. 1997 Waves, turbulence and entrainment near an inversion layer. *J. Fluid Mech.* Submitted for publication.

Carruthers, D. J., Hunt, J. C. R. & Turfus, C. J. 1986 Turbulent flow near density inversion layers. In *Proc. Euromech Colloquium 199* (ed. U. Schumann & R. Friedrich), pp. 271–290. Friedr. Vieweg & Sohn.

Carruthers, D. J. & Moeng, C.-H. 1987 Waves in the overlying inversion of the convective boundary layer. *J. Atmos. Sci.* **44**, 1801–1808.

Caughey, S. J., Crease, B. A. & Roach, W. T. 1982 A field study of nocturnal stratocumulus, II. *Q. R. Met. Soc.* **198**, 124–144.

Caughey, S. J. & Palmer, S. G. 1979 Some aspects of turbulence through the depth of the convective boundary layer. *Q. J. R. Met. Soc.* **105**, 495–527.

Chase, D. M. 1970 Space-time correlations of velocity and pressure and the role of convection for homogeneous turbulence in the universal range. *Acustica* **22**, 303–320.

Courant, R. & Hilbert, D. 1953 *Methods of Mathematical Physics*, vol. 1, Interscience.

Crapper, P. F. & Linden, P. F. 1974 The structure of the turbulent density interfaces. *J. Fluid Mech.* **65**, 45–83.

Davis, R. E. & Acrivos, A. 1967 The stability of oscillatory internal waves. *J. Fluid Mech.* **30**, 723–736.

Deardorff, J. W. 1980 Stratocumulus-capped mixed-layers derived from a three-dimensional model. *Boundary-Layer Met.* **18**, 495–527.

Desaubies, Y. & Smith, W. K. 1982 Statistics of Richardson number and instability in oceanic waves. *J. Phys. Oceanogr.* **12**, 1245–1287.

E, X. & Hopfinger, E. J. 1986 On mixing across an interface in stably stratified fluid. *J. Fluid Mech.* **166**, 227–244.

Fernando, H. J. S. 1989 Buoyancy transfer across a diffusive interface. *J. Fluid Mech.* **209**, 1–34.

Fernando, H. J. S. 1991 Turbulent mixing in stratified flows. *Ann. Rev. Fluid Mech.* **23**, 455–493.

Fernando, H. J. S. 1995 Migration of density interfaces subjected to differential turbulent mixing. *J. Geophys. Astrophys. Fluid Dyn.* **78**, 1–20.

Fernando, H. J. S. & Long, R. R. 1985 On the nature of the entrainment interface of a two-layer fluid subjected to zero-mean-shear turbulence. *J. Fluid Mech.* **151**, 21–53.

Fleury, M., Mory, M., Hopfinger, E. J. & Auchere, D. 1991 Effects of rotation on turbulent mixing across a density interface. *J. Fluid Mech.* **223**, 165–191.

Fung, J. C. H., Hunt, J. C. R., Malik, N. A. & Perkins, R. J. 1992 Kinematic simulation of homogeneous turbulent flows generated by unsteady random Fourier modes. *J. Fluid Mech.* **236**, 281–318.

Gill, A. E. 1982 *Atmosphere-Ocean Dynamics*. Academic.

Hannoun, I. A. 1987 Turbulent mixing in stably stratified fluids. PhD thesis, California Institute of Technology.

Hannoun, I. A., Fernando, H. J. S. & List, E. J. 1988 Turbulence structure near a sharp density interface. *J. Fluid Mech.* **189**, 189–209.

Hannoun, I. A. & List, E. J. 1988 Turbulent mixing at a shear-free density interface. *J. Fluid Mech.* **189**, 211–234.

Hopfinger, E. J. & Toly, J. A. 1976 Spatially decaying turbulence and its relation to mixing across density interfaces. *J. Fluid Mech.* **78**, 155–175.

Hunt, J. C. R. 1973 A theory of turbulent flow round two-dimensional bluff bodies. *J. Fluid Mech.* **61**, 625–706.

Hunt, J. C. R. 1984 Turbulence structure in thermal convection and shear-free boundary layers. *J. Fluid Mech.* **138**, 161–184.

Hunt, J. C. R. & Carruthers, D. J. 1990 Rapid distortion theory and the 'problem' of turbulence. *J. Fluid Mech.* **212**, 497–532.

Hunt, J. C. R., Fung, J. C. H., Malik, N. A., Perkins, R. J., Vassilicos, J. C., Wray, A. A., Buell, J. C. & Bertoglio, J. P. 1991 Kinematics of small scale motions in homogeneous isotropic turbulence. In *Advances in Turbulence III* (ed. A. V. Johansson & P. H. Alfredsson). Springer.

Hunt, J. C. R., Stretch, D. D. & Britter, R. E. 1986 Length-scales in stably stratified turbulent flows and their use in turbulence models. *Proc. IMA Conf. on Stably Stratified Flows and Dense-gas Dispersion.* Clarendon.

Huppert, H. E., Turner, J. S. & Hallworth, M. A. 1995 Sedimentation and entrainment in dense layers of suspended particles stirred by an oscillating grid. *J. Fluid Mech.* **289**, 263–293.

Huq, P. & Britter, R. E. 1995 Turbulence evolution and mixing in a two-layer stably stratified fluid. *J. Fluid Mech.* **285**, 41–67.

Jayesh & Warhaft, Z. 1994 Turbulent penetration of a thermally stratified interfacial layer in a wind tunnel. *J. Fluid Mech.* **277**, 23–54.

Jayesh, Yoon, K. & Warhaft, Z. 1991 Turbulent mixing and transport in a thermally stratified interfacial layer in decaying grid turbulence. *Phys. Fluids* A **3**, 1143–1155.

Kelley, D. 1987 Interfacial migration in thermohaline staircases. *J. Phys. Oceanogr.* **17**, 1633–1639.

Kit, E., Fernando, H. J. S. & Brown, J. A. 1995 Experimental examination of Eulerian frequency spectra in zero-mean-shear turbulence. *Phys. Fluids* **7**, 1168–1170.

Kit, E., Strang, E. J. & Fernando, H. J. S. 1997 Measurement of zero mean shear turbulence in homogenous two-layer fluids. *J. Fluid Mech.* **334**, 293–314.

Lenschow, D. H., Patel, V. & Isbell, A. 1988 Measurement of fine structure at the top of marine stratocumulus. *Proc. 8th Symp. on Turbulence and Diffusion, San Diego, CA*, pp. 29–32.

Lewellen, W. S. & Sykes, R. I. 1982 A numerical study of breaking Kelvin–Helmholtz billows using a Reynolds-stress closure model. *J. Atmos. Sci.* **39**, 1506–1520.

Linden, P. F. 1973 The interaction of vortex rings with a sharp density interface: a model for turbulent entrainment. *J. Fluid Mech.* **60**, 467–480.

Linden, P. F. 1975 The deepening of a mixed layer in a linearly stratified fluid. *J. Fluid Mech.* **71**, 385–405.

Linden, P. F. 1979 Mixing in stratified fluids. *Geophys. Astrophys. Fluid Dyn.* **13**, 2–23.

Linden, P. F. 1980 Mixing across a density interface produced by grid turbulence. *J. Fluid Mech.* **100**, 691–703.

Long, R. R. 1978 A theory of mixing in a stably stratified fluid. *J. Fluid Mech.* **84**, 113–124.

McEwan, A. D. 1983 The kinematics of stratified mixing through internal wave breaking. *J. Fluid Mech.* **128**, 47–58.

McGrath J., Fernando, H. J. S. & Hunt, J. C. R. 1997 Turbulence, waves and mixing at shear-free density interfaces. Part 2. Laboratory experiments. *J. Fluid Mech.* **347**, 235–261.

Moeng, C.-H. 1986 A large-eddy simulation study of stratus-topped boundary layer. *J. Atmos. Sci.* **43**, 2886–2900.

Moffatt, H. K. 1984 Simple topological aspects of turbulent velocity dynamics. *Proc. IUTAM Symp. on Turbulence and Chaotic Phenomena in Fluids* (ed. T. Tatsumi). Elsevier.

Mory, M. 1991 Models of turbulent mixing at a density interface including the effects of rotation. *J. Fluid Mech.* **223**, 193–207.

Nokes, R. I. 1988 On the entrainment across a density interface. *J. Fluid Mech.* **188**, 185–204.

Pearson, H. M. J., Puttock, J. S. & Hunt, J. C. R. 1983 A statistical model of fluid element motions and vertical diffusion in a homogeneous stratified turbulent flow. *J. Fluid Mech.* **29**, 219–249.

Perera, M. J. A. M., Fernando, H. J. S. & Boyer, D. L. 1994 Turbulent mixing at an inversion layer. *J. Fluid Mech.* **267**, 275–298.

Phillips, O. M. 1977 *Dynamics of the Upper Ocean*, 2nd edn. Cambridge University Press.

Redondo, J. 1990 Topics on dense-gas dispersion and turbulent mixing at density interfaces. PhD thesis, University of Cambridge.

Siegel, D. A. & Domaradzki, A. J. 1994 Large eddy simulation of decaying stably stratified turbulence. *J. Phys. Oceanogr.* **24**, 2253–2286.

Tennekes, H. 1975 Eulerian and Lagrangian time microscales in isotropic turbulence. *J. Fluid Mech.* **67**, 561–567.

Tennekes, H. & Lumley, J. L. 1973 *A First Course in Turbulence*. MIT Press.

Thompson, J. M. T. 1989 Chaotic phenomena triggering the escape from a potential well. *Proc. R. Soc. Lond.* A **421**, 195–225.

Thompson, R. O. R. Y. 1984 Formation of thermoclines in zero-mean-shear turbulence. *J. Geophys. Res.* **89**, 8017–8021.

Thompson, S. M. & Turner, J. S. 1975 Mixing at an interface due to turbulence generated by an oscillating grid. *J. Fluid Mech.* **67**, 349–368.

Thorpe, S. A. 1985 Laboratory observations of secondary structures in Kelvin–Helmholtz billows and consequences for ocean mixing. *Geophys. Astrophys. Fluid Dyn.* **34**, 175–199.

Turner, J. S. 1968 The influence of molecular diffusivity on turbulent entrainment across a density interface. *J. Fluid Mech.* **33**, 639–656.

Turner, J. S. 1986 Turbulent entrainment: the development of the entrainment assumption, and its application to geophysical flows. *J. Fluid Mech.* **173**, 431–471.

Wijesekera, H. W., Dillon, T. M. & Padman, L. 1993 Some statistical and dynamical properties of turbulence in the oceanic pycnocline. *J. Geophys. Res.* **98**, 22665–22679.